ELSEVIER

PII: S0266-3538(96)00140-6

Composites Science and Technology **58** (1998) 1045–1067

Printed in Great Britain
0266-3538/98 $—see front matter

FAILURE ANALYSIS OF FRP LAMINATES BY MEANS OF PHYSICALLY BASED PHENOMENOLOGICAL MODELS*

A. Puck & H. Schürmann†

University of Technology Darmstadt, Fachgebiet Konstruktiver Leichtbau und Bauweisen, 30 Petersenstrasse, 64287 Darmstadt, Germany

(Received 9 August 1995; revised 11 April 1996; accepted 11 September 1996)

Abstract

A realistic failure analysis of structural members made of FRP composites requires consideration of the non-linear stress/strain relationships. In laminate design and for determination of safety factors of FRP structural members, there is a strong need for fracture criteria and degradation models which are simple enough for application in common engineering problems while still being in good agreement with physical reality. It is essential to distinguish between fibre failure and inter-fibre failure by separate failure criteria. A recent success was the introduction of inter-fibre failure criteria which model the brittle failure behaviour of composites very realistically. These not only provide realistic stresses to failure, but also indicate the crack direction, which is an extremely important piece of information when evaluating the likely effect of fracture. After crack initiation, the stiffnesses of the affected plies degrade gradually with increasing load, until fibre fracture in one ply provokes ultimate failure of the laminate. Also, an inclined wedge-shaped inter-fibre crack can lead to ultimate failure. From now on, the risk of fracture caused by these phenomena can be evaluated. The determination of the fracture angle which is the key for this evaluation is derived in the present paper. © *1998 Elsevier Science Ltd. All rights reserved*

Keywords: laminate design, non-linear stress/strain behaviour, failure criteria, fracture angle, degradation model

NOTATION

Characteristics of the unidirectional layer

x_1, x_2, x_3	Coordinate system of a unidirectional layer (x_1 = fibre direction, x_3 = thickness direction)
$\sigma_1, \sigma_2, \sigma_3$	Normal stresses in a unidirectional layer
$\tau_{12} = \tau_{21}; \tau_{13} = \tau_{31}; \tau_{23} = \tau_{32}$	Shear stresses of a unidirectional layer in the elastic symmetry directions. The first subscript indicates the direction normal to the plane on which the shear stress is acting; the second subscript indicates the direction of the shear force.
$\epsilon_1, \epsilon_2, \epsilon_3$	Normal strains of a unidirectional layer
$\gamma_{12} = \gamma_{21}; \gamma_{13} = \gamma_{31}; \gamma_{23} = \gamma_{32}$	Shear strains of a unidirectional layer
$\sigma_\parallel; \sigma_\perp$	Stressing parallel and transverse to the fibre direction
$\tau_{\perp\parallel}; \tau_{\perp\perp}$	Shear stressing transverse/parallel and transverse/transverse to the fibre direction
$E_1, E_2 = E_3$	Elastic moduli of a unidirectional layer in the directions x_1, x_2, x_3
$E_{1t}, E_{2t}, E_{3t}; E_{1s}, E_{2s}, E_{3s}$	Tangent moduli, secant moduli
$G_{21}; G_{21s}$	Shear modulus of a unidirectional layer in the x_2, x_1 direction; secant shear modulus
ν_{12}	Major Poisson's ratio
$X_T; X_C$	Tensile strength and compressive strength of the unidirectional layer parallel to the fibre direction
$Y_T; Y_C$	Tensile strength and compressive strength of the unidirectional layer transverse to the fibre direction
S_{21}	Shear strength of a unidirectional layer transverse and parallel to the fibre direction

Characteristics of the fibres

$\sigma_{f1}; \sigma_{f2}$	Fibre stress in x_1 direction; fibre stress in x_2 direction
E_{f1}	Fibre modulus in x_1 direction
ν_{f12}	Poisson's ratio of the fibres (strain in x_2 direction caused by a stress in the x_1 direction)

*This article represents the authors' contributions to a worldwide exercise to confirm the state-of-the-art for predicting failure in composites, organised by Hinton and Soden.[24]

†To whom correspondence should be addressed.

ϵ_{1T}; ϵ_{1C}	Tensile failure strain and compression failure strain of a unidirectional layer in x_1 direction
X_{fT}; X_{fC}	Tensile fibre strength and compressive fibre strength in fibre direction (in a UD composite)
$m_{\sigma f}$	Mean stress magnification factor for the fibres in the x_2 direction, due to the difference between the transverse modulus of the fibre and the modulus of the matrix

Characteristics of the potential fracture plane

x_1,x_n,x_t	Coordinate system rotated with respect to the fibre direction by an angle θ from the x_2 direction to the x_n direction
σ_n	Normal stress acting on the potential fracture plane
τ_{nt}	Normal/transverse shear stress acting on the potential fracture plane
τ_{n1}	Normal/longitudinal shear stress acting on the potential fracture plane
R^A	Fracture resistance of a stress action plane against its own fracture caused by one single stress acting in it
$R_{\perp}^{(+)A}$	Fracture resistance of the action plane against its fracture due to transverse tensile stressing
$R_{\perp\perp}^{A}$	Fracture resistance of the action plane against its fracture due to transverse/transverse shear stressing
$R_{\perp\parallel}^{A}$	Fracture resistance of the stress action plane against its fracture due to transverse/parallel shear stressing
θ	Angle between the x_2 axis and the x_n axis
θ_{fp}	Angle of the fracture plane
$p_{\perp\parallel}^{(-)}$	Slope of the (σ_n, τ_{n1}) fracture envelope for $\sigma_n \leq 0$ at $\sigma_n = 0$
$p_{\perp\perp}^{(-)}$	Slope of the (σ_n, τ_{nt}) fracture envelope for $\sigma_n \leq 0$ at $\sigma_n = 0$
f_w	Weakening factor due to the degrading influence of high σ_1 stresses
σ_{1d}	Emperical stress value, determining the degradation of the fracture resistance R^A of the action plane due to σ_1 stresses ($\sigma_{1d} > 0$ for $\sigma_1 > 0$; $\sigma_{1d} < 0$ for $\sigma_1 < 0$)
σ_{1D}	Stress value for linear degradation ($\sigma_{1D} > 0$ for $\sigma_1 > 0$; $\sigma_{1D} < 0$ for $\sigma_1 < 0$)
$f_R(\theta)$	Angle-dependent reserve factor, stretching factor for the applied stress state which is necessary to achieve IFF at θ
$f_{E_{(IFF)}}$	Angle-dependent effort of a unidirectional layer with respect to IFF (see *Abbreviations*)
τ_{21c}	Shear stress at the 'turning point' of the (σ_2,τ_{21}) fracture curve
$\sigma^{(l)},\tau^{(l)}$; $\sigma^{(r)},\tau^{(r)}$	Load-dependent stress; residual stress
$\eta = \eta f_{E_{(IFF)}}$	Degradation factor representing reduction of transverse stiffness due to inter-fibre fracture

Abbreviations

CLT	Classical laminate theory
FF	Fibre failure
FPF	First ply failure
FRP	Fibre reinforced plastic
IFF	Inter-fibre fracture

1 INTRODUCTION

Strength analysis of laminates is still underdeveloped compared to the analysis of stresses and strains. Specifically, there is a lack of fracture criteria and degradation models which are both close to physical reality and simple enough for application in engineering design of laminates with optimum strength. Few of the present models meet both requirements.

Significant characteristics of the fracture criteria and degradation models presented in this paper were already described more than 25 years ago in two publications.[1,2] The most important statements of these papers were:

- Two basically independent fracture criteria have to be applied simultaneously: one for fibre failure (FF), and one for inter-fibre failure (IFF), because the effects of both fracture phenomena are totally different, as well as the design methods to avoid one or the other failure.
- The (σ_2, τ_{21}) failure envelope should not be described by a single equation, which includes both the transverse tensile strength, Y_T, and the transverse compression strength, Y_C. The reason for this is that the strength characteristics in the compression domain $(\sigma_2 < 0)$ are independent of the tensile strength, and the strength characteristics in the tension domain $(\sigma_2 > 0)$ are also independent of the compressive strength.
- Stiffness degradation by smearing of the cracks after crack initiation should be continuous instead of sudden. Additionally, it has to be applied selectively for $(\sigma_2 < 0)$ different from that for $(\sigma_2 > 0)$.

- When judging the significance of IFF, one has to be careful to distinguish between the fairly harmless crack formation caused by transverse tensile stresses ($\sigma_2 > 0$), compared to the 'explosive' effect that oblique cracks, caused by transverse compressive stresses ($\sigma_2 < 0$), have because of their wedge shape.

On the basis of these principal findings, numerous details of the fracture criteria have been improved in the past; specifically, the extension of the fracture criteria for a three-dimensional state of stress has to be mentioned.[3,4]

IFF criteria, in particular, have been significantly improved recently by placing them on a solid physical basis[5–10]; an extensive coverage of these new developments has been given previously.[11]

Many efforts were made during recent years to describe the complex damage and fracture phenomena of composites physically in correct ways, i.e. in many cases by means of fracture mechanics, and the new research field of damage mechanics has rapidly grown up.[12] The results of this approach provide important insights into micromechanical behaviour; however, for application in current engineering design they still seem to be inappropriate. Three different kinds of models for the description of damage and fracture behaviour have been used hitherto:

(a) micromechanical models,
(b) probabilistical models,
(c) phenomenological models.

In the present paper, phenomenological models are applied, but they are placed on a solid physical basis. They not only provide results for the stress level which leads to crack initiation and to fracture, but also indicate the direction of the cracks. Nevertheless, their application is surprisingly simple and therefore provide an interesting opportunity for use in everyday engineering design.

In principle, damage and fracture analysis of laminates requires the following:

1. analysis of strains and stresses ply by ply;
2. fracture criteria for single plies;
3. degradation models to include the effects of partial fracture, which often does not lead to ultimate failure of the laminate;
4. a computer program which simulates the gradual fracture process by applying the above sequences iteratively.

In the following, these four considerations are discussed in succession. According to the problems of the Failure Analysis Exercise,[24,25] the discussion is limited to a state of plane stress ($\sigma_1, \sigma_2, \tau_{21}$).

2 REMARKS ON THE ANALYSIS OF STRAINS AND STRESSES

For the analysis of strains and stresses of single plies the well-known classical laminate theory (CLT) is used. However, for application in fracture analysis of FRP laminates it has to be modified in order to include the non-linear relationships between stress and strain. These non-linear effects can be observed, especially in (τ_{21}, γ_{21}) diagrams, but also in (σ_2, ϵ_2) diagrams if σ_2 is a compressive stress.

Several opportunities to include non-linear effects exist, but not all of them are equally practical. Generally, it is assumed that the non-linear stress/strain relationships remain unchanged, no matter whether the load is σ_1 alone, σ_2 alone, τ_{21} alone, or a superposition of all three stresses. This means, for example, that a (τ_{21}, γ_{21}) diagram remains unchanged when, in addition to a τ_{21} stress, a σ_2 stress is superimposed which is proportional to τ_{21}.

This is not found in reality, as can be concluded from the stress/strain diagrams under several different loading combinations (σ_2, τ_{21})[13] (Fig. 1). The additional microdamage which is caused by the σ_2 load leads to a shallower (τ_{21}, γ_{21}) curve than with τ_{21} load alone and *vice versa*.

Our computer program makes it possible to take such interactions between the stresses σ_2 and τ_{21} into account. However, in order to do this some stress/strain diagrams for combined (σ_2, τ_{21}) loading must be available, which is not the case for the laminates which have to be analysed in the problems given in this exercise. Generally, it should be pointed out that neglecting the interaction in combined (σ_2, τ_{21}) loading results in calculating a level of crack initiation which is too low.

For calculation of the stresses σ_2 or τ_{21}, respectively, on the basis of experimentally determined (σ_2, ϵ_2) or (τ_{21}, γ_{21}) diagrams, it is possible to use either tangent moduli $E_{2t} = \mathrm{d}\sigma_2/\mathrm{d}\epsilon_2$ or secant moduli $E_{2s} = \sigma_2/\epsilon_2$ for instance. Calculation with secant moduli is more practical, since the tangent modulus method normally requires many sufficiently small calculation steps, starting from zero load, before the final stress/strain state can be reached, whereas the secant modulus method allows one to reach this point with one large load step and only a few iterations. Figure 2 shows this for a τ_{21} load.

Furthermore, the secant modulus method offers the advantage of being self-correcting. With increasing load, the making of a mistake when computing the stress for a certain load level does not change the calculated stress state for a higher load level. In contrast, when the tangent modulus method is used, the current stress is always the sum of many $\Delta\sigma$, so that mistakes add up.

For τ_{21} shear stresses, it is irrelevant whether the secant modulus, G_{21s}, is taken at the shear stress, τ_{21}, or at the shear strain, γ_{21}. However, when calculating with

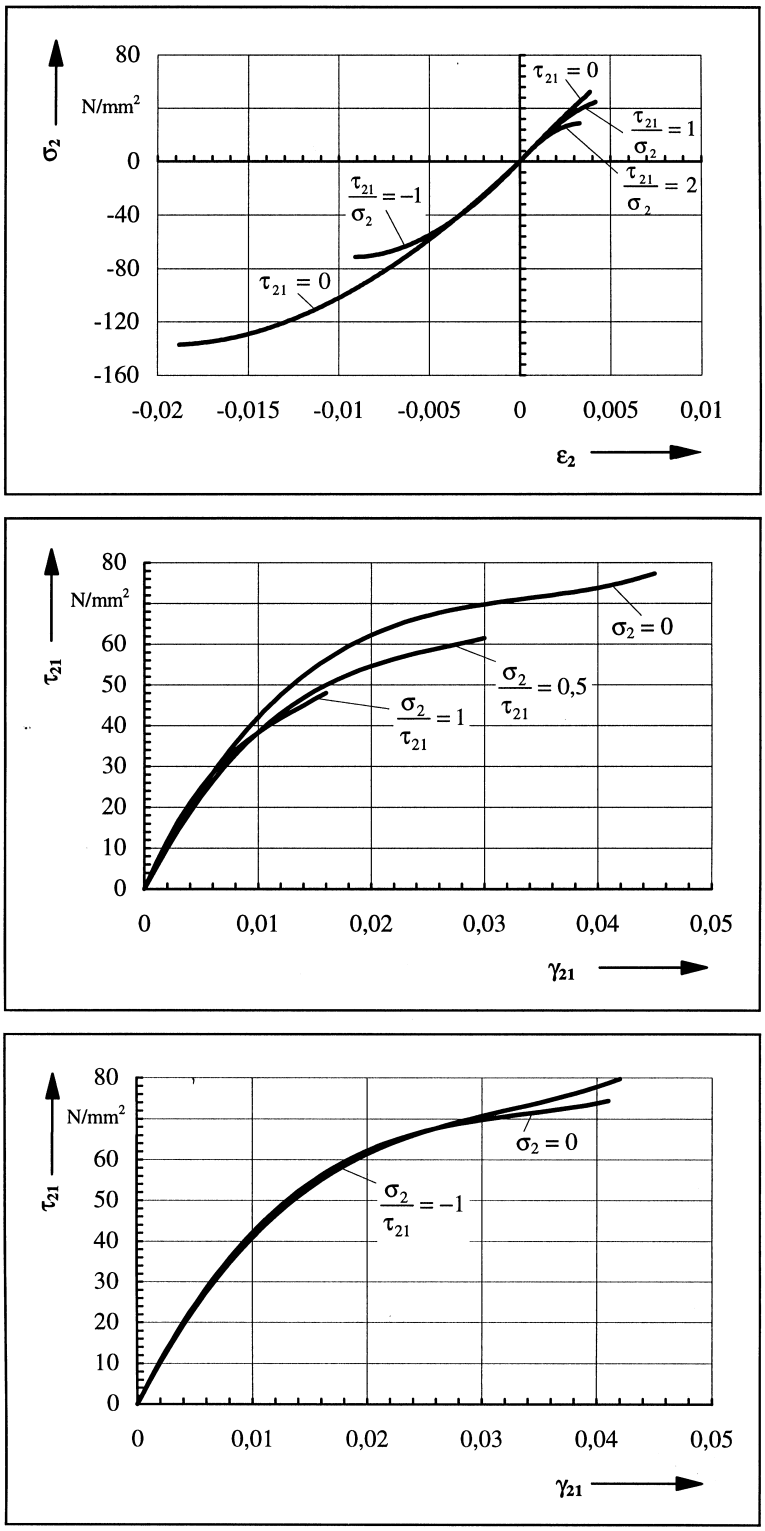

Fig. 1. Stress/strain diagrams of glass-fibre/epoxy UD specimens under combined (σ_2,τ_{21}) loading.

non-linear (σ_2, ϵ_2) relationships and σ_1 and σ_2 are acting simultaneously, the secant modulus can only be deduced at the calculated stress σ_2, and not at the calculated strain ϵ_2, since the strain ϵ_2 is dependent not only on the stress σ_2, but also on the stress σ_1 because of transverse contraction (Poisson's effect) (Fig. 3).

In our program, all stress/strain curves are approximated by spline functions of third order. Calculation above crack initiation level might require an extrapolation of the (σ_2, ϵ_2) or (τ_{21}, γ_{21}) diagrams beyond the fracture point. Nevertheless, the method of performing the stress analysis after crack initiation exactly can only

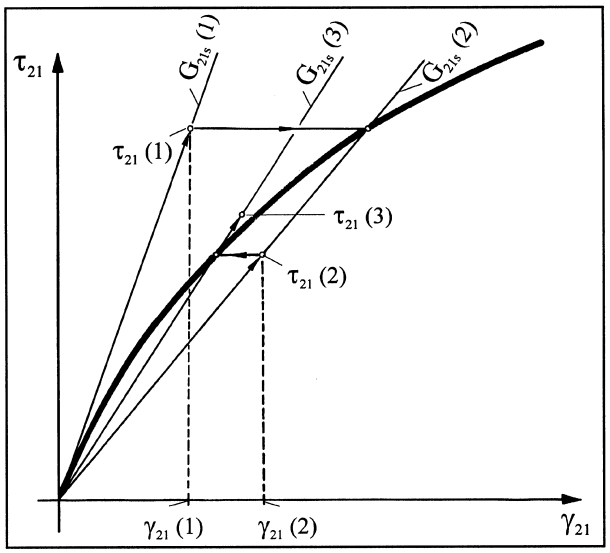

Fig. 2. Calculating stress and strain of a UD layer with non-linear (τ_{21},γ_{21}) behaviour by iteration.

be explained after having described the selected degradation model.

3 FAILURE CONDITIONS FOR FIBRE FAILURE (FF)

Up to now, a state of stress is regarded as being the limit for fibre failure in a unidirectional composite when, under combined loading, a stress σ_1 parallel to the fibres evolves which is equal to the longitudinal strength (tensile strength X_T or compressive strength X_C) determined by a uniaxial test. Correspondingly, a failure condition for the strain ϵ_1 which is parallel to the fibres of a unidirectional laminate is formulated: ϵ_1 must be equal to the longitudinal fracture strain, ϵ_{1T} or ϵ_{1C}.[3,4] In reality, the truth lies between these two approaches, as shown in the following.

Fundamentally, we assume that fibre failure in a UD composite under a combined state of stress $(\sigma_1, \sigma_2, \sigma_3, \tau_{23}, \tau_{31}, \tau_{21})$ will occur at the same fibre stress as that which is acting in the fibres at failure under a unaxial stress σ_1. Starting from this failure hypothesis we have to begin with a failure condition for the fibre instead of for the unidirectional composite:

$$\sigma_{f1} = X_{fT} \quad \text{for} \quad \sigma_{f1} \geq 0 \tag{1}$$

$$\sigma_{f1} = -X_{fC} \quad \text{for} \quad \sigma_{f1} < 0 \tag{2}$$

By this it is assumed that for the fibre, the failure condition of the maximum normal stress in the fibre direction holds. It should be pointed out that X_{fT} and X_{fC} are the tensile stress or the compressive stress in the fibre which are reached under uniaxial tensile or compressive load with σ_1 at fracture of the unidirectional composite material and not in single fibres or fibre bundles. Assuming linear-elastic material behaviour, these are given by:

$$X_{fT} = \frac{X_T}{E_1} E_{f1} = \epsilon_{1T} E_{f1} \text{ and } X_{fC} = \frac{X_C}{E_1} E_{f1} = \epsilon_{1C} E_{f1} \tag{3}$$

While X_{fT} can be regarded as the 'true' tensile strength of the fibre (embedded in the composite), X_{fC} is usually not the 'true' compressive strength of the fibre, because at $\sigma_{f1} < 0$, failure mostly occurs through elastic instability (so-called microbuckling or kinking) of the fibres embedded elastically in the matrix. However, it can be assumed that the buckling is not influenced by an additional stress σ_2, at most by an additional stress τ_{21}.[14] Thus, X_{fC} can be regarded as a constant.

Already at a state of stress where $\sigma_1 = 0$, but $\sigma_2 \neq 0$, stresses of opposite sign occur in fibres and matrix in a direction parallel to the fibres because of their different elastic moduli and Poisson's ratios (for $\sigma_2 > 0$ it is

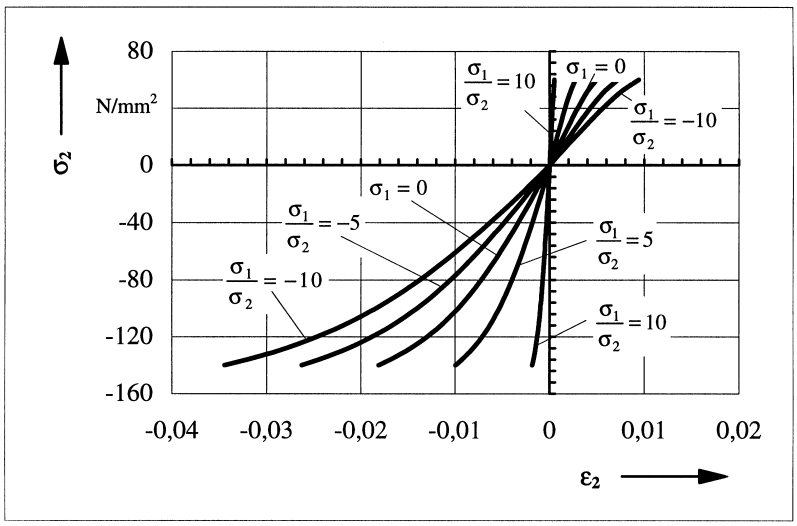

Fig. 3. Changing of the (σ_2, ϵ_2) curve caused by the simultaneous action of a stress σ_1.

$\sigma_{f1} < 0$ and for $\sigma_2 < 0$ it is $\sigma_{f1} > 0$). This is taken into account by the equation:

$$\epsilon_{f1} = \frac{\sigma_{f1}}{E_{f1}} - \frac{\nu_{f12}}{E_{f1}} m_{\sigma f} \sigma_2 \tag{4}$$

The factor $m_{\sigma f}$ accounts for a 'stress magnification effect' caused by the different moduli of fibres and matrix (in the σ_2 direction), which leads to an uneven distribution of the stress σ_2 from a micromechanical point of view: in the fibres, it is slightly higher than in the matrix. The factor $m_{\sigma f}$ is a mean magnification factor m of the transverse stress (index σ) for the fibre (index f) (for glass fibre $m_{\sigma f} \approx 1.3$; for carbon fibre $m_{\sigma f} \approx 1.1$).

Because of the tight bonding between fibres and matrix, the strain parallel to the fibres is the same for the fibres and the composite:

$$\epsilon_{f1} = \epsilon_1 \tag{5}$$

Thus, the longitudinal stress in the fibre σ_{f1} under combined $(\sigma_{f1}, \sigma_{f2})$ loading is obtained from eqn (4) as:

$$\sigma_{f1} = \epsilon_1 E_{f1} + \nu_{f12} m_{\sigma f} \sigma_2 \tag{6}$$

When this stress reaches the same stress level, σ_1, the fibre is subjected to at fracture of the unidirectional composite under uniaxial tension or compression, the fibre breaks:

$$\sigma_{f1} = \epsilon_{1T} E_{f1} \text{ or } \sigma_{f1} = -\epsilon_{1C} E_{f1} \tag{7}$$

Therefore, on the basis of the failure hypothesis mentioned, the failure condition for fibre failure under combined $(\sigma_{f1}, \sigma_{f2})$ loading is:

$$\frac{1}{\epsilon_{1T}} \left(\epsilon_1 + \frac{\nu_{f12}}{E_{f1}} m_{\sigma f} \sigma_2 \right) = 1 \text{ for } (\ldots) \geq 1 \tag{8}$$

$$\frac{1}{\epsilon_{1C}} \left(\epsilon_1 + \frac{\nu_{f12}}{E_{f1}} m_{\sigma f} \sigma_2 \right) = -1 \text{ for } (\ldots) < 1 \tag{9}$$

when the fracture strain ϵ_{1C} is written as a positive value.

In a previous publication[15] it was emphasised that experimental results show that the compressive strength, X_C, parallel to the fibres and, consequently, also $_{1C}$ are significantly reduced, when in addition to $\sigma_1 < 0$, a significant shear stress, τ_{21}, is superimposed. This can be explained by the observation that a τ_{21} load promotes fibre kinking by compression parallel to the fibres. Edge noted an interaction equation,[15] which yields $X_{1C} = 0$ when τ_{21} reaches the inter-fibre failure limit, i.e. $\tau_{21} = S_{21}$. This is in contrast with our experimental experience: if a unidirectional ply in a laminate is already damaged by cracks caused by τ_{21} loading, it can still transfer significant σ_1 compressive stresses. Therefore, we are using an empirical shear correction substantially lower than the one described by Edge:

$$\frac{1}{\epsilon_{1C}} \left| \left(\epsilon_1 + \frac{\nu_{f12}}{\epsilon_{f1}} m_{\sigma f} \sigma_2 \right) \right| + (10\gamma_{21})^2 = 1 \text{ for } (\ldots) < 0 \tag{10}$$

where $(10\gamma_{21})^2$ is a pure empirical approach. It is preferable to use an expression with γ_{21} instead of τ_{21}, because the value of τ_{21} is uncertain after crack initiation while the value of γ_{21} is not.

It has been pointed out[16] that X_{1C} significantly increases when a hydrostatic pressure $\sigma_2 = \sigma_3$ acts at the same time. It is still not clear whether this effect also takes place when $\sigma_2 \neq 0$ and $\sigma_3 = 0$. Thus, we do not include any further interactions between σ_1 and σ_2 at fibre failure than the ones mentioned above.

It should be mentioned that Hart-Smith[17] contradicts the failure hypothesis of the constant longitudinal stress of the fibres. He assumes a distinct reduction of X_1, when the fibres suffer approximately equal strains but with opposite sign, in the longitudinal and transverse direction: this must be studied in more depth.

4 FAILURE CONDITIONS FOR INTER-FIBRE FAILURE (IFF)

In this research field, the greatest improvements have been achieved recently.[5–8] The knowledge gained by experiments with carbon-fibre/epoxy and glass-fibre/epoxy laminates (which are to be analysed in this paper) teaches that unidirectional layers behave in a very brittle manner at failure, particularly at inter-fibre failure. Without any previous macromechanically apparent plastic deformation, abrupt material separation occurs when the specimen reaches the point of failure.[9] Considering this observation, it seems surprising that many scientists, when implementing failure criteria for brittle composites, decided to follow the yield criteria of von Mises or Hill which hold only for ductile materials. It seems much more appropriate to use the failure criteria of Mohr[18] as guidelines, these having been developed for materials that exhibit brittle fracture characteristics. This idea was originally formulated, to the knowledge of the authors, by Hashin.[19] He stated that transferring the fracture criteria of Mohr on unidirectional composites would put fibre failure criteria and inter-fibre failure criteria on a solid physical basis. Hashin never accomplished his idea, however, considering the computational effort to be far too great. However, the enormously increased computer capacities which are nowadays available for almost every design engineer make it desirable to develop and apply these ideas further.[5] The current achievements are extensively discussed elsewhere.[11]

Surprisingly, it has recently been found that application of new fracture criteria which are based on physical

foundations not only provides additional information about the angle of fracture, but also needs only little computer capacity when limited to a state of plane stress (σ_1, σ_2, τ_{21}), compared to the capacity required by currently used failure criteria. Therefore, in this paper we already apply the new failure criteria, which are briefly explained in the following; a broad coverage can be found elsewhere.[11]

Like Mohr, we proceed on the hypothesis that fracture is exclusively created by the stresses which act on the fracture plane. In the case of inter-fibre fracture on an inclined plane parallel to the fibres these are a normal stress, σ_n, and two shear stresses, τ_{nt} and τ_{n1} (Fig. 4). The stress σ_n represents a transverse stressing ($\sigma_\perp$), the shear stress τ_{nt} a transverse–transverse shear stressing $\tau_{\perp\perp}$ and the shear stress τ_{n1} a transverse–longitudinal shear stressing ($\tau_{\perp\parallel}$). The term 'stressing' has been introduced by Puck[11] in order to distinguish between stress conditions of different character, e.g. $\sigma_\parallel$, $\sigma_\perp$, $\tau_{\perp\perp}$, $\tau_{\perp\parallel}$

When $\sigma_n > 0$, i.e. transverse tensile stressing, it causes fracture in conjunction with τ_{nt} and τ_{n1}. Because of the existing symmetry, the direction of the shear stresses cannot influence fracture.[11] The simplest approach one can think of for $\sigma_n \geq 0$ would consequently be:[5,19]

$$\left(\frac{\sigma_n}{R_\perp^{(+)A}}\right)^2+\left(\frac{\tau_{nt}}{R_{\perp\perp}^{A}}\right)^2+\left(\frac{\tau_{n1}}{R_{\perp\parallel}^{A}}\right)^2 = 1 \text{ for } \sigma_n \geq 0 \qquad (11)$$

In this equation, generally the common strengths cannot be used in the denominators. This can easily be seen when recalling the fundamental hypothesis: fracture of the plane in which the stresses act which cause fracture is exclusively created by the stresses which act in this plane. Consequently, the three stresses σ_n, τ_{nt}, τ_{n1}, which must necessarily have a common stress action plane, must be compared to the fracture resistances R^A (A representing action plane) of their action plane, and not just to some strength which might belong to any other fracture plane. If a stress $\sigma_n > 0$ is acting alone and fracture occurs in its stress action plane, the fracture resistance $R_\perp^{(+)A}$ equals the tensile strength Y_T. This is the case with the UD materials of laminates examined here, which does not mean that it is so in general. However, a $\tau_{\perp\parallel}$ shear stressing always causes fracture only in its action plane;[11] thus, we can write $R_{\perp\parallel}^{A} = S_{21}$. With $R_{\perp\perp}^{A}$, the situation is totally different for the materials to be analysed. A shear stressing $\tau_{\perp\perp}$ which acts alone does not lead to shear fracture in its action plane, but to tensile fracture in a plane which is inclined by 45° to the action plane of the shear stress. Up to now, no experiment is known which would allow a direct measurement of the fracture resistance $R_{\perp\perp}{}^{A}$ against fracture caused by a $\tau_{\perp\perp}$ stressing. Hence, $R_{\perp\perp}{}^{A}$ has to be derived from the transverse compressive strength, Y_C, assuming a mathematically formulated master fracture surface (see Table 1).

The unusual part of the new fracture criteria can be seen in their definition in the (σ_n, τ_{nt}, τ_{n1}) stress space. Still, stress analysis gives the existing stresses in the (x_1, x_2, x_3) coordinate system, which is dependent on the fibre direction and the mid-plane of the unidirectional ply. From the (σ_1,σ_2,σ_3,τ_{23},τ_{31},τ_{21}) stress space, one gets into the (σ_n,τ_{nt},τ_{n1}) stress space (Fig. 4) through the well-known transformation rules, which are for a state of plane (σ_1,σ_2,τ_{21}) stress:

$$\begin{aligned} \sigma_1 &= \sigma_1 \\ \sigma_n &= \sigma_2 \cos^2\theta \\ \tau_{nt} &= -\sigma_2 \sin\theta\cos\theta \\ \tau_{n1} &= \tau_{21}\cos\theta \end{aligned} \qquad (12)$$

Generally, the calculation procedure is now to insert the stresses (σ_n, τ_{nt}, τ_{n1}), which are in terms of σ_1, σ_2, τ_{21} and θ, in a fracture condition like eqn (11). The angle θ_{fp} (fp represents failure plane) then has to be determined

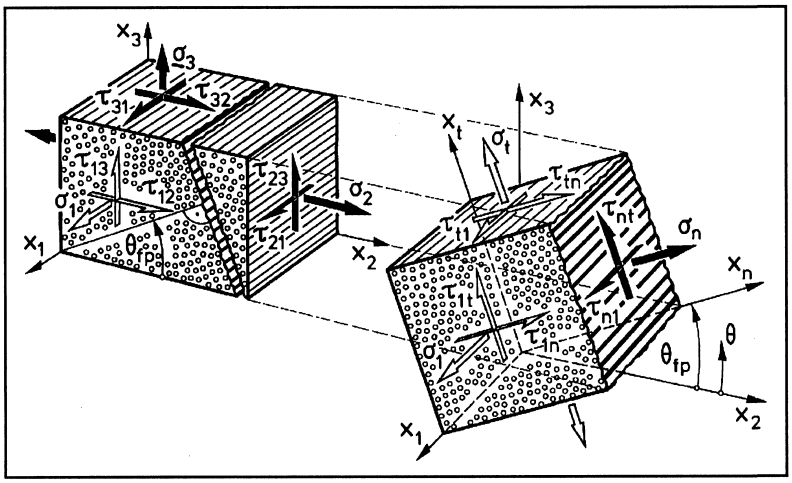

Fig. 4. Three-dimensional stresses on a UD composite element. (x_1,x_2,x_3) coordinate system is fixed to fibre direction (x_1), laminate mid-surface (x_2) and thickness direction (x_3). The (x_1,x_n,x_t) coordinate system is rotated by an angle θ_{fp} from the x_2 direction to the x_n direction which is normal to the fracture plane. The inter-fibre fracture is influenced by the the three stresses σ_n, τ_{nt}, τ_{n1} only (according to Mohr's strength theory).

for which the risk of fracture in the related stress action plane (θ) has its global maximum. With θ_{fp} being determined by this condition, the stresses (σ_n, τ_{nt}, τ_{n1}) at fracture can be calculated, together with the reserve factor, f_R, which is the factor all existing stresses have to be multiplied with in order to achieve fracture. The reserve factor, f_R, is the same for the stresses (σ_n, τ_{nt}, τ_{n1}) as well as for (σ_1,σ_2,σ_3,τ_{23},τ_{31},τ_{21}) because of eqn (12).

A tensile stress $\sigma_n > 0$ promotes fracture, whereas a compressive stress $\sigma_n < 0$ impedes shear fracture. For $\sigma_n < 0$, the shear stresses τ_{nt} and τ_{n1} (or just one of them) have to cause fracture against an additional fracture resistance, which increases with increasing $|\sigma_n|$ like an internal friction. A simple approach describing this effect is performed by the following equation,[11,20] which resembles the fracture hypothesis by Mohr–Coulomb:[21]

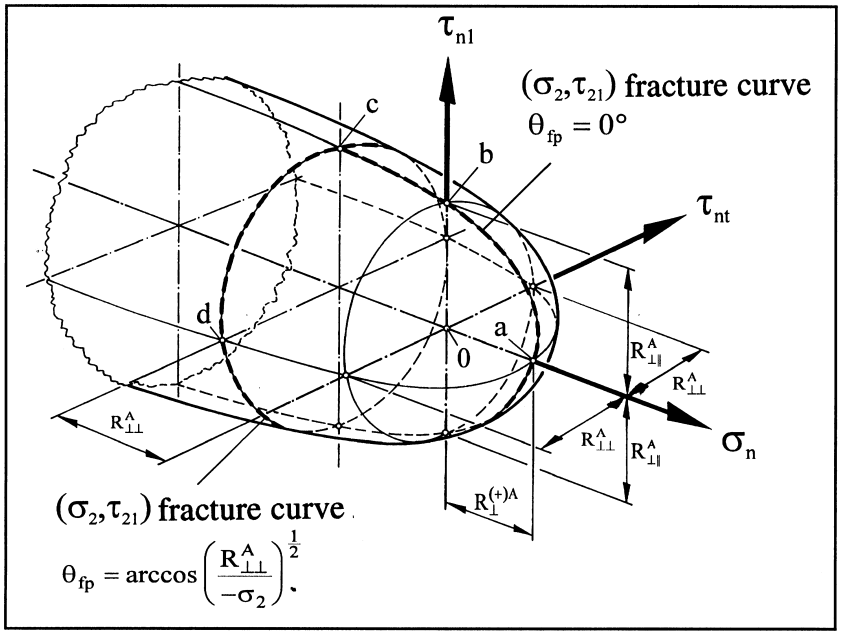

Fig. 5. Master fracture surface (for $\sigma_1 = 0$) for UD material in the (σ_n,τ_{nt},τ_{n1}) stress space with fracture resistances $R_{\perp}^{(+)A}$, $R_{\perp\parallel}^{A}$, $R_{\perp\perp}^{A}$ of the stress action plane. If there is a degradation effect of σ_1, all dimensions have to be reduced by $f_w = 1 - (\sigma_1/\sigma_{1d})^n = 1 - |\sigma_1/\sigma_{1D}|$. The ($\sigma_2$,$\tau_{21}$) fracture curve follows a contour line (from a to c) and then a boundary line of a cross-section (from c to d). Compare with Fig. 6.

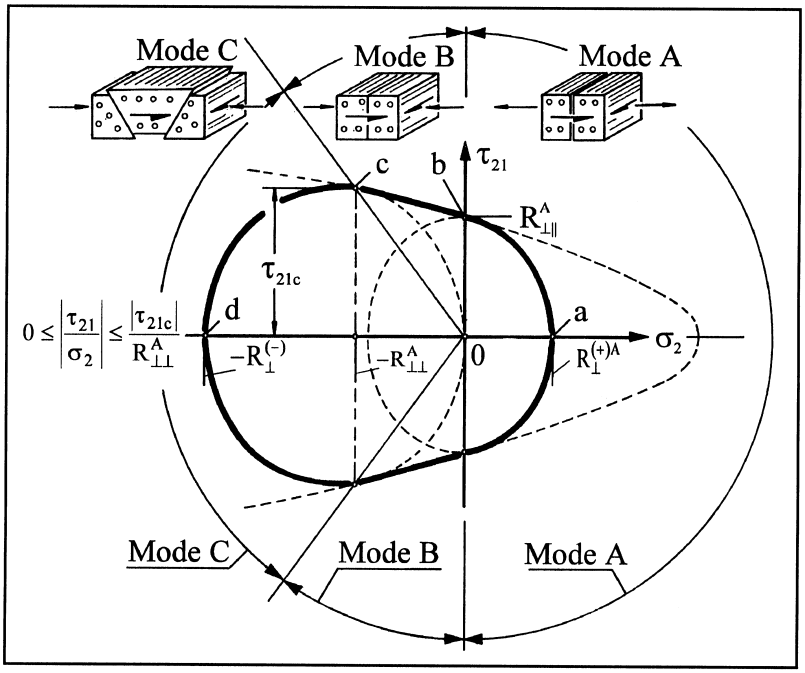

Fig. 6. (σ_2,τ_{21}) fracture curve for $\sigma_1 = 0$, representing three different fracture modes A, B, C. The curve is generated by two ellipses and one parabola. If a degradation by σ_1 takes place, the fracture curve shrinks by a factor f_w under the condition of geometric similarity.

$$\left(\frac{\tau_{nt}}{R^{A}_{\perp\perp} - p^{(-)}_{\perp\perp}\sigma_n}\right)^2 + \left(\frac{\tau_{n1}}{R^{A}_{\perp\parallel} - p^{(-)}_{\perp\parallel}\sigma_n}\right)^2 = 1 \text{ for } \sigma_n < 0 \quad (13)$$

Both fracture conditions, eqns (11) and (13), have been further modified to achieve a better agreement with experimental results:[11]

$$c_2\left(\frac{\sigma_n}{R^{(+)A}_{\perp}}\right)^2 + c_1\frac{\sigma_n}{R^{(+)A}_{\perp}} + \left(\frac{\tau_{nt}}{R^{A}_{\perp\perp}}\right)^2 + \left(\frac{\tau_{n1}}{R^{A}_{\perp\parallel}}\right)^2 = 1 \text{ for } \sigma_n \geq 0 \quad (14)$$

$$\frac{\tau^2_{nt}}{(R^{A}_{\perp\perp})^2 - 2p^{(-)}_{\perp\perp}R^{A}_{\perp\perp}\sigma_n} + \frac{\tau^2_{n1}}{(R^{A}_{\perp\parallel})^2 - 2p^{(-)}_{\perp\parallel}R^{A}_{\perp\parallel}\sigma_n} = 1 \text{ for } \sigma_n < 0 \quad (15)$$

These two equations are the basis for the inter-fibre fracture condition worked out in this paper.

An essential simplification is performed in eqn (15) by coupling the thus far independent slopes $p^{(-)}_{\perp\perp}$ and $p^{(-)}_{\perp\parallel}$. To calculate eqn (15) with reasonable computational effort, we assume in this paper that the following coupling exists:

$$\frac{p^{(-)}_{\perp\perp}}{R^{A}_{\perp\perp}} = \frac{p^{(-)}_{\perp\parallel}}{R^{A}_{\perp\parallel}} = \left(\frac{p}{R}\right) = \text{const.} \quad (16)$$

This simplification seems to be acceptable according to our experience. In general, $p^{(-)}_{\perp\parallel}$ is fitted to the experimentally deduced slope of the (σ_2,τ_{21}) fracture envelope for $\sigma_2 \leq 0$ at the point $\sigma_2 = 0$, so that $p^{(-)}_{\perp\perp} = p^{(-)}_{\perp\parallel}R^{A}_{\perp\perp}/R^{A}_{\perp\parallel}$ is fixed as well.

With the assumption made in eqn (16), eqn (15) reduces to a much simpler form:

$$\left(\frac{\tau_{nt}}{R^{A}_{\perp\perp}}\right)^2 + \left(\frac{\tau_{n1}}{R^{A}_{\perp\parallel}}\right)^2 + 2\left(\frac{p}{R}\right)\sigma_n = 1 \text{ for } \sigma_n < 0 \quad (17)$$

The fracture body described by eqns (14) and (17) in the $(\sigma_n, \tau_{nt}, \sigma_{nl})$ stress space is an ellipsoid on the tensile side $\sigma_n \geq 0$ and a paraboloid (with parabolic contours and elliptical cross-sections) on the compression side $\sigma_n < 0$. The surface of this fracture body will be referred to as the master fracture surface (Fig. 5).

In accordance with experimental findings, applying eqn (14) for the special case of plane stress (σ_2,τ_{21}) gives anywhere for $\sigma_2 \geq 0$ a fracture angle $\theta_{fp} = 0°$. Recalling the transformation rules (eqn (12)) with

$$\sigma_n = \sigma_2;\ \tau_{nt} = 0;\ \tau_{nl} = \tau_{21}$$

the fracture condition eqn (14) reduces to

$$c_2\left(\frac{\sigma_2}{R^{(+)A}_{\perp}}\right)^2 + c_1\frac{\sigma_2}{R^{(+)A}_{\perp}} + \left(\frac{\tau_{21}}{R^{A}_{\perp\parallel}}\right)^2 = 1 \text{ for } \sigma_2 \geq 0 \quad (18)$$

As described in full detail elsewhere[11] we finally arrive at:

$$\sqrt{\left(\frac{\tau_{21}}{R^{A}_{\perp\parallel}}\right)^2 + \left(1 - \frac{p^{(+)}_{\perp\parallel}}{R^{A}_{\perp\parallel}}R^{(+)A}_{\perp}\right)^2\left(\frac{\sigma_2}{R^{(+)A}_{\perp}}\right)^2} + \frac{p^{(+)}_{\perp\parallel}}{R^{A}_{\perp\parallel}}\sigma_2 = 1 \text{ for } \sigma_2 \geq 0 \quad (19)$$

The fracture mechanism described by eqn (19), where σ_2 and/or τ_{21} cause fracture, will be called Mode A (Fig. 6).

Applying eqn (17) to the domain of $\sigma_2 < 0$, it can be found that also on the compression side there is a part of the fracture envelope where the fracture angle $\theta_{fp} = 0°$. Fracture is originated by τ_{21}, whereas σ_2 impedes fracture. The τ_{21} stress at fracture increases parabolically with increasing compressive stress. In eqn (17), $\tau_{nt} = 0$, $\tau_{nl} = \tau_{21}$ and $\sigma_n = \sigma_2$ is assigned. Again, like eqn (19), a fracture condition can be found which is homogeneous and of first degree in terms of stresses:[11]

$$\sqrt{\left(\frac{\tau_{21}}{R^{A}_{\perp\parallel}}\right)^2 + \left(\frac{p}{R}\right)^2\sigma_2^2} + \left(\frac{p}{R}\right)\sigma_2 = 1 \text{ for } \sigma_2 < 0 \quad (20)$$

This fracture mechanism is called Mode B (Fig. 6).

In fracture tests under uniaxial transverse compressive load it can be observed that fracture angles $\theta_{fp} \approx \pm 45°$ appear, with $|\theta_{fp}|$ usually slightly higher than 45°.[9] Consequently, it can be anticipated that the fracture angle ,θ_{fp}, in the course of the (σ_2,τ_{21}) fracture envelope somewhere between the shear strength $R_{\perp\parallel}$ and the compressive strength $R^{(-)}_{\perp}$ changes from $\theta_{fp} = 0°$ (in Mode B) to values $\theta_{fp} \neq 0°$. For a closer examination, the fracture condition of eqn (17) has to be implemented for every possible fracture angle $-90° \leq \theta \leq +90°$ to detect the stress action plane with the highest risk of fracture.

For a general three-dimensional stress state $(\sigma_1,\sigma_2,\sigma_3,\tau_{23},\tau_{31},\tau_{21})$ (Fig. 4), determination of the fracture angle is only possible by numerical procedures. For that purpose, the program FRACUAN (fracture curves analysis) was developed at the University of Kassel, Germany (Department of Mathematics, Working Group Engineering Mathematics, Mrs Prof. Dr R. Jeltsch-Fricker; MS Thesis D. Zeise, University of Kassel, 1993). Among other things, the program calculates the shape of the risk-of-fracture curve for $-90° \leq \theta \leq +90°$. The risk of fracture is defined as the angle-dependent effort $f_E(\theta)$ for a given stress state and any angle θ between $-90°$ and $+90°$. The risk of fracture or angle-dependent effort is the reciprocal value of the angle-dependent reserve factor $f_R(\theta)$. $f_R(\theta)$ is the positive stretching factor which would be necessary to increase a given state of stress $(\sigma_1,\sigma_2,\sigma_3,\tau_{23},\tau_{31},\tau_{21})$ so much that it leads to fracture in the sectional plane (θ) of interest. The minimal stretching factor $[f_R(\theta)]_{min} = f_R(\theta_{fp})$ which occurs in the angle range $-90° \leq \theta \leq +90°$ at the angle θ_{fp} is the conventional generally used reserve factor, f_R.

For the cutting angle θ_{fp} which belongs to the minimal angle-dependent reserve factor $f_R(\theta_{fp})$ the actual fracture can be expected, because at this angle the risk of fracture is highest.

One of the computational results of FRACUAN deserves particular interest: applying the fracture models in eqn (13) or eqn (15), respectively, and assuming that eqn (16) is valid for (σ_2,τ_{21}) stress states, the normal stress σ_n on the fracture plane is constant on all inclined fracture planes ($\theta_{fp}\neq 0$) . This observation suggests a further analytical investigation.

Therefore, we consider a $(\sigma_1,\sigma_2,\tau_{21})$ state of stress in the range $\sigma_2<0$ which leads to IFF.[11] At the moment of fracture, two conditions are satisfied:

1. Fracture occurs in the one sectional plane where the angle-dependent effort $f_E(\theta)$ is a maximum, i.e.

$$\frac{d}{d\theta}(f_E(\theta))=0 \tag{21}$$

2. The fracture condition is satisfied, i.e.

$$f_E(\theta_{fp})=1-\frac{\sigma_1}{\sigma_{1D}}=f_w \tag{22}$$

In this case it is necessary already to introduce the weakening factor f_w, which describes a certain degradation of the fracture resistances of the action plane by high σ_1 stresses (see Section 7.1).

The fracture condition can be expressed as a function of $\cos\theta$. Therefore, expanding eqn (21) gives:

$$\begin{aligned}\frac{d}{d\theta}(f_E(\theta))&=\frac{d}{d(\cos\theta)}(f_E(\theta))\frac{d}{d\theta}(\cos\theta)\\&=\frac{d}{d(\cos\theta)}(f_E(\theta))(-\sin\theta)=0\end{aligned}$$

The first solution for this equation is $\theta_{fp}=0°$, which was already used when describing the fracture mechanism referred to as Mode B.

A second solution can be expected from

$$\frac{d}{d(\cos\theta)}(f_E(\theta))=0$$

To find the solution, we start with an alternative form of the fracture condition which follows from eqn (17), in which the value of the function on the left-hand side of the equation increases proportionally with the stress level.[11] Thus, this alternative form cannot only be used to formulate the fracture condition, but also to calculate the effort:

$$\begin{aligned}f_E(\theta_{fp})&=\sqrt{\left(\frac{\tau_{nt}}{R^A_{\perp\perp}}\right)^2+\left(\frac{\tau_{nl}}{R^A_{\perp\parallel}}\right)^2+\left(\frac{p}{R}\right)^2\sigma_n^2}+\left(\frac{p}{R}\right)\sigma_n \\&=f_w \quad \text{for} \quad \sigma_n<0\end{aligned} \tag{23}$$

In accordance with the transformation rules in eqn (12), this equation may be written for an arbitrary angle θ as:

$$\begin{aligned}f_E(\theta)=&\\&\cos(\theta)\sqrt{\left(\frac{\sigma_2}{R^A_{\perp\perp}}\right)^2(1-\cos^2\theta)+\left(\frac{\tau_{21}}{R^A_{\perp\parallel}}\right)^2+\left(\frac{p}{R}\right)^2\sigma_2^2\cos^2\theta}\\&+\left(\frac{p}{R}\right)\sigma_2\cos^2\theta+\frac{\sigma_1}{\sigma_{1D}} \quad \text{for} \quad \sigma_n<0\end{aligned}$$

Introducing the abbreviations

$$\begin{aligned}a=\left[\left(\frac{p}{R}\right)^2-\left(\frac{1}{R^A_{\perp\perp}}\right)^2\right]\sigma_2^2;\ b=\left(\frac{\tau_{21}}{R^A_{\perp\parallel}}\right)^2\\+\left(\frac{\sigma_2}{R^A_{\perp\perp}}\right)^2;\ c=\left(\frac{p}{R}\right)\sigma_2\end{aligned}$$

the angle-dependent effort becomes a function of $\cos\theta$ of the form

$$f_E(\theta)=\cos\theta\sqrt{a\cos^2\theta+b}+c\cos^2\theta+\frac{\sigma_1}{\sigma_{1D}}$$

It follows from eqn (21) and its first solution $\theta_{fp}=0°$ that

$$\begin{aligned}\frac{d}{d(\cos\theta)}(f_E(\theta))=&\sqrt{a\cos^2\theta_{fp}+b}\\&+\frac{a\cos^2\theta_{fp}}{\sqrt{a\cos^2\theta_{fp}+b}}+2c\cos\theta_{fp}=0\end{aligned} \tag{24}$$

Since the fracture situation is considered, the fracture condition also holds:

$$f_E(\theta_{fp})=\cos\theta_{fp}\sqrt{a\cos^2\theta_{fp}+b}+c\cos^2\theta_{fp}=f_w$$

Using this equation, the 'unpleasant' square root in the derivation can be eliminated, which finally gives:

$$\begin{aligned}\cos^4\theta&=\frac{f_w^2}{c^2-a}\\\theta_{fp}&=\arccos\sqrt{\frac{f_w R^A_{\perp\perp}}{(-\sigma_2)}}\end{aligned} \tag{25}$$

In eqn (25) σ_2 is the stress at inter-fibre fracture. By this, it is possible to determine the fracture angle, θ_{fp}, (with validity of eqns (15) and (16)) in a surprisingly simple way.

It can be shown, moreover, that the normal stress σ_n in the fracture plane is constant in the whole range where inclined fracture planes occur, because it is $\sigma_n=\sigma_2\cos^2\theta_{fp}=-f_w R^A_{\perp\perp}$. It is therefore not dependent on the stress ratio τ_{21}/σ_2. Between $\sigma_2=0$ and $\sigma_2=-f_w R^A_{\perp\perp}$, the fracture angle is $\theta_{fp}=0°$, and the normal stress is given by $\sigma_2=\sigma_n$. When the compressive

stress exceeds the value of $-f_w R^A_{\perp\perp}$, the fracture plane surprisingly always turns exactly so much that $\sigma_n = \sigma_2 \cos^2 \theta_{fp}$ remains constant.

On the master fracture surface (Fig. 5), the fracture curve for a (σ_2,τ_{21}) load, starting from point (a) for pure $\sigma_\perp$ tension passing point (b) for pure $\tau_{\perp\parallel}$ shear up to the turning point (c) follows a longitudinal section contour line, and from (c) to (d) for pure $\sigma_\perp$ compression a cross-section contour line of the master fracture body.

Knowing the fracture angle θ_{fp}, eqn (17) or eqn (23) yield the fracture condition for inclined fracture through a (σ_2,τ_{21}) load:

$$\frac{1}{2\left[1+\left(\frac{p}{R}\right)R^A_{\perp\perp}\right]}\left[\left(\frac{\tau_{21}}{R^A_{\perp\parallel}}\right)^2+\left(\frac{\sigma_2}{R^A_{\perp\perp}}\right)^2\right]\frac{R^A_{\perp\perp}}{(-\sigma_2)} + \frac{\sigma_1}{\sigma_{1D}} = 1 \quad \text{for} \quad \sigma_2 < 0 \tag{26}$$

This equation may be written in many variations. One which is particularly simple results from the relation between $R^A_{\perp\perp}$ and the transverse compressive strength Y_C; this is given in Table 1. The associated fracture mechanism is called Mode C (Fig. 6).

5 SURVEY OF FRACTURE CONDITIONS AND RELATIONSHIPS BETWEEN SUBSTANTIAL PARAMETERS

Table 1 summarises all fracture conditions used in this paper in a clearly arranged manner. The fracture resistances R^A of the stress action plane are already replaced by the strength values Y_T, Y_C and S_{12} as far as possible.

By an additional term f_w, a possible influence of the stress σ_1 parallel to the fibres on the inter-fibre failure can be included. This is explained in detail in Section 7.1 which deals with degradation by σ_1 stresses.

Regarding the physically-based inter-fibre fracture conditions given in Table 1, it is obvious that they do not require more computational effort than the present, widely used, fracture criteria. Thus, the only supplementary task is to decide which equation is valid for the stress state to be analysed. However, distinguishing between Mode A, B or C is easily possible, considering the criteria given in Table 1 (see also Fig. 6).

As a result, it can be seen that with remarkably little extra work, one gets important additional information about the fracture mode and the anticipated fracture angle, which brings along a much better assessment of the consequences that inter-fibre failures may have for the laminate.

6 RESERVE FACTOR AND EFFORT IN THE PRESENCE OF RESIDUAL STRESSES

When no residual stresses exist, the following definition is valid:

(a) The reserve factor f_R is the one (positive) factor all existing stresses would have to be multiplied with to originate failure. This means that the stress vector would have to be stretched in its original direction by this factor in order to cause fracture.

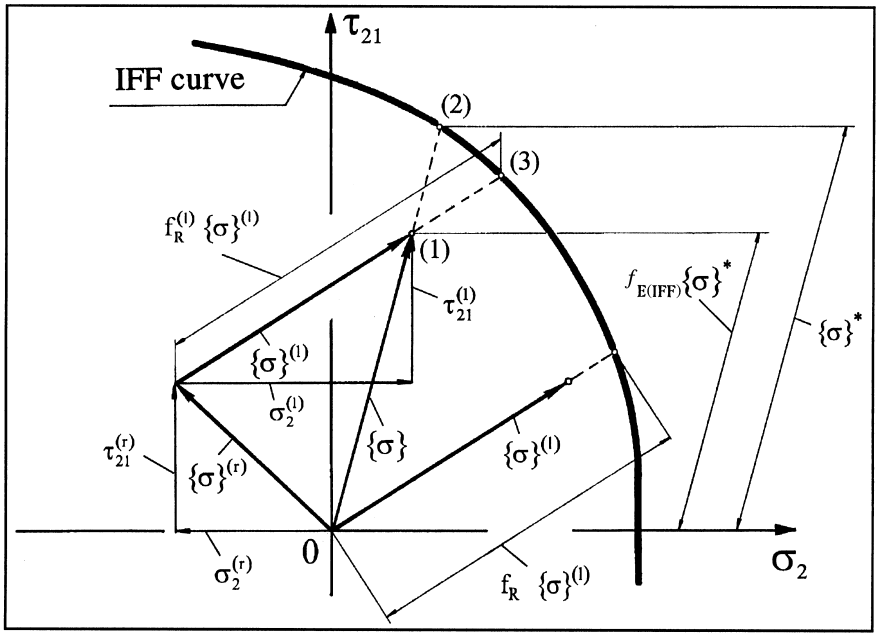

Fig. 7. Stress vectors in the (σ_2,τ_{21}) plane with and without a residual stress $\{\sigma\}^{(r)}$. Illustration of reserve factors f_R, $f_R^{(1)}$ and the inter-fibre failure effort $f_{E(IFF)}$. (1) Tip of the resultant stress vector $\{\sigma\}$; (2) stretching of $\{\sigma\}$ until IFF occurs; (3) stretching of the load-dependent stress vector $\{\sigma\}^{(I)}$ until IFF occurs.

Table 1. Summary of failure conditions (for the calcuation of $f_{E(FF)}$ or $f_{E(IFF)}$ the terms with γ_{21} or σ_1, respectively, have to be shifted to the left-hand side)

Type of failure	Failure mode	Failure condition (effort $f_{E(FF)}$ or $f_{E(IFF)}$)	Condition for validity
Fibre failure (FF)	Tensile	$\frac{1}{\epsilon_{1T}}\left(\epsilon_1 + \frac{\nu_{f12}}{E_{f1}} m_{\sigma f}\sigma_2\right) = 1$	$(\ldots)\geq 0$
	Compression (kinking)	$\frac{1}{\epsilon_{1C}}\left\|\left(\epsilon_1 + \frac{\nu_{f12}}{E_{f1}} m_{\sigma f}\sigma_2\right)\right\| = 1 - (10\gamma_{21})^2$	$(\ldots) < 0$
Inter-fibre fracture (IFF)	Mode A, $\theta_{fp} = 0°$	$\sqrt{\left(\frac{\tau_{21}}{S_{21}}\right)^2 + \left(1 - p^{(+)}_{\perp\parallel}\frac{Y_T}{S_{21}}\right)^2\left(\frac{\sigma_2}{Y_T}\right)^2} + p^{(+)}_{\perp\parallel}\frac{\sigma_2}{S_{21}} = 1 - \left\|\frac{\sigma_1}{\sigma_{1D}}\right\|$	$\sigma_2 \geq 0$
	Mode B, $\theta_{fp} = 0°$	$\frac{1}{S_{21}}\left(\sqrt{\tau_{21}^2 + \left(p^{(-)}_{\perp\parallel}\sigma_2\right)^2} + p^{(-)}_{\perp\parallel}\sigma_2\right) = 1 - \left\|\frac{\sigma_1}{\sigma_{1D}}\right\|$	$\sigma_2 < 0$ and $0 \leq \left\|\frac{\sigma_2}{\tau_{21}}\right\| \leq \frac{R^A_{\perp\perp}}{\lvert\tau_{21c}\rvert}$
	Mode C, $\cos\theta_{fp} = \sqrt{\frac{f_w R^A_{\perp\perp}}{(-\sigma_2)}}$	$\left[\left(\frac{\tau_{21}}{2(1+p^{(-)}_{\perp\perp})S_{21}}\right)^2 + \left(\frac{\sigma_2}{Y_C}\right)^2\right]\frac{Y_C}{(-\sigma_2)} = 1 - \left\|\frac{\sigma_1}{\sigma_{1D}}\right\|$	$\sigma_2 < 0$ and $0 \leq \left\|\frac{\tau_{21}}{\sigma_2}\right\| \leq \frac{\lvert\tau_{21c}\rvert}{R^A_{\perp\perp}}$
Definitions	$p^{(+)}_{\perp\parallel} = -\left(\frac{d\tau_{21}}{d\sigma_2}\right)_{\sigma_2=0}$ of (σ_2, τ_{21}) curve, $\sigma_2 \geq 0$	$p^{(-)}_{\perp\parallel} = -\left(\frac{d\tau_{21}}{d\sigma_2}\right)_{\sigma_2=0}$ of (σ_2, τ_{21}) curve, $\sigma_2 \leq 0$	
Parameter relationships	$R^A_{\perp\perp} = \frac{Y_C}{2(1+p^{(-)}_{\perp\perp})} = \frac{S_{21}}{2p^{(-)}_{\perp\parallel}}\left(\sqrt{1 + 2p^{(-)}_{\perp\parallel}\frac{Y_C}{S_{21}}} - 1\right)$	$p^{(-)}_{\perp\perp} = p^{(-)}_{\perp\parallel}\frac{R^A_{\perp\perp}}{S_{21}}$	$\tau_{21c} = S_{21}\sqrt{1 + 2p^{(-)}_{\perp\perp}}$

In Fig. 7, such an increase of stresses can be seen in the stretching of the stress vector $\{\sigma\}^{(1)}$.

If residual stresses (index r) $\{\sigma\}^{(r)}$ exist, it is only possible to define a reserve factor of the load dependent stresses (index l) $\{\sigma\}^{(l)}$:

(a) The reserve factor $f_R^{(l)}$ of the load-dependent stresses is the one (positive) factor all load dependent stresses would have to be multiplied with to cause fracture.

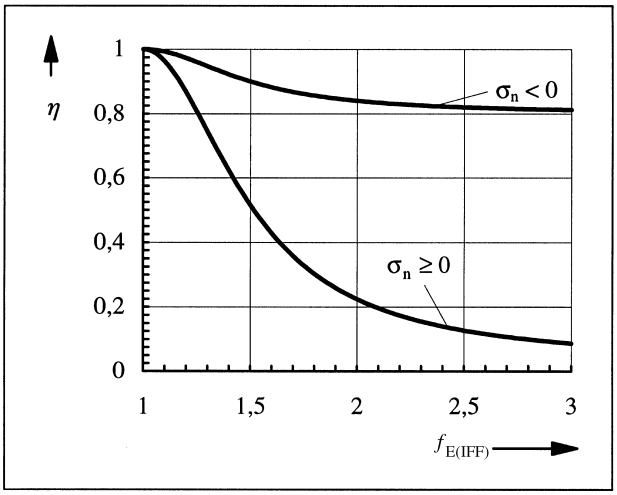

Fig. 8. Degradation factor η as a function of the calculated $f_{E(IFF)} > 1$ above the fracture limit ($f_{E(IFF)} = 1$) of a UD layer.

If no residual stresses exist, the inverse value $(f_R)^{-1}$ is the factor of effort or, abbreviated, the effort f_E.

With acting residual stresses, the effort is not the reciprocal value $(f_R^{(l)})^{-1}$, but the reciprocal value of that factor by which the resulting stress vector $\{\sigma\} = \{\sigma\}^{(r)} + \{\sigma\}^{(l)}$ would have to be multiplied with (maintaining its direction) to cause fracture (compare (1)→(2) and (1)→(3) in Fig. 7).

Defining a reserve factor $f_R^{(l)}$ for the load dependent stresses is reasonable (see Fig. 7), whereas introducing an 'effort factor' for the load dependent stresses $\{\sigma\}^{(l)}$ does not make sense.

For a plane $(\sigma_1,\sigma_2,\tau_{21})$ state of stress, the existing stresses are:

$$\sigma_1 = \sigma_1^{(r)} + \sigma_1^{(l)};\ \sigma_2 = \sigma_2^{(r)} + \sigma_2^{(l)};\ \tau_{21} = \tau_{21}^{(r)} + \tau_{21}^{(l)} \qquad (27)$$

To determine the fibre failure effort $f_{E(FF)}$ or the inter-fibre failure effort $f_{E(IFF)}$, respectively, which belong to a particular stress state, the stresses σ_1, σ_2, τ_{21} calculated according to eqn (27) are inserted in the fracture conditions summarised in Table 1. These stresses either do not lead to fracture, or already exceeded the fracture limit. Inserting these stresses on the left-hand side of the fracture condition gives a number which is the value of the effort $f_{E(FF)}$ or $f_{E(IFF)}$, respectively. (The term (σ_1/σ_{1D}) has to be shifted to the left-hand side.) This comes from the fact that the functions characterising

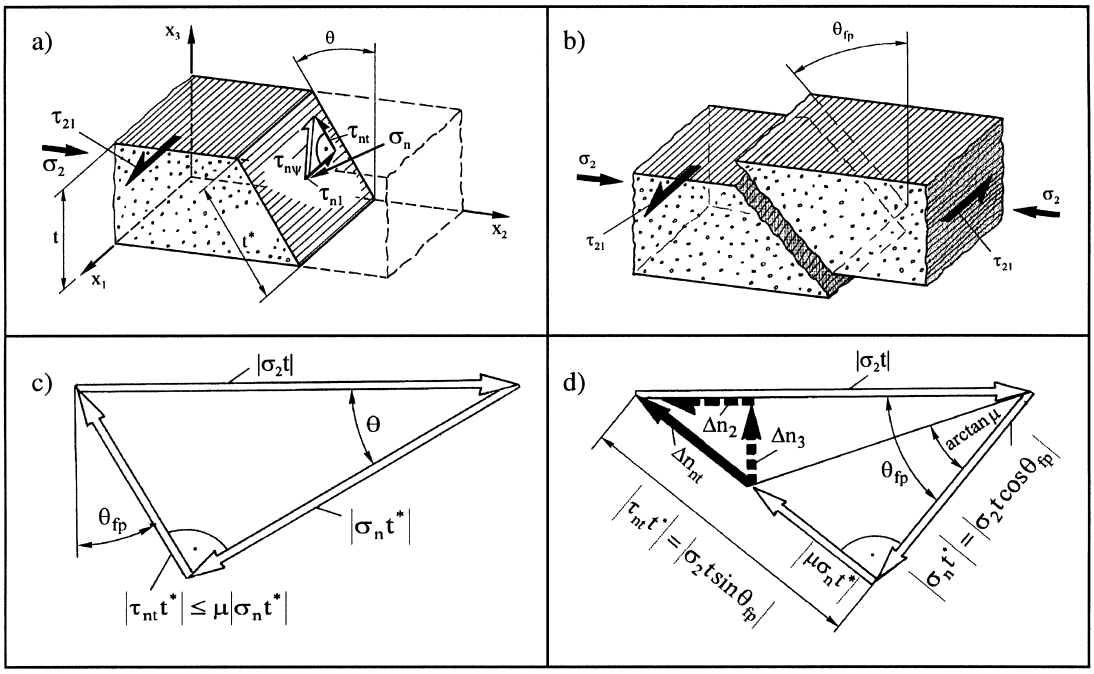

Fig. 9. Wedge effect of inclined mode C fracture planes caused by $(\sigma_1,\sigma_2,\tau_{21})$ stresses. (a) Stress state on an inclined cut under the angle θ: normal stress σ_n. The shear stresses τ_{nt} and τ_{n1} may be combined to $\tau_{n\psi}$. (b) If $\tau_{n\psi}t^*$ exceeds the maximum friction force $\mu\sigma_n t^*$, the fractured pieces glide one against the other in the $\tau_{n\psi}$ direction. (c) Equilibrium of forces on a fragmented piece $\tau_{21} = \tau_{n1} = 0$; as long as $|\tau_{nt}t^*|$ remains lower than the maximum possible friction force $\mu|\sigma_n t^*|$, the fractured pieces do not glide. (d) Forces acting on fractured piece with large fracture angle θ_{fp}; $\tau_{21} = \tau_{n1} = 0$. The maximum friction force has been exceeded. Within a laminate the surplus force Δn_2 will be introduced by an interlaminar shear stress τ_{32} into the neighbouring layers. Δn_3 produces, by interlaminar normal stresses, an explosive effect on the laminate.

fracture on the left-hand side of the fracture condition are homogeneous of first degree in terms of stresses.[11]

Certainly an influence of loading path on the IFF strength can be expected, but we are not able to take this into consideration. We have to apply the same IFF curve for stress vectors with and without residual stresses.

7 DEGRADATION MODELS

7.1 Degradation of fracture resistances in the inter-fibre fracture conditions due to single fibre failure

Since fibre strength follows a statistical distribution, single fibres already break under uniaxial σ_1 tensile stress long before fracture of many fibres leads to ultimate failure when X_T is reached. These preliminary single fibre breaks cause local damage in the vicinity of the breaks in the form of debonding of fibre and matrix and microcracks in the matrix. By this damage the fracture resistances R^A the composite offers to inter-fibre fracture are decreased. This is taken into account by equally decreasing all fracture resistances R^A with a weakening factor f_w.[11] In order to keep the fracture conditions homogeneous and of first degree with respect to the stresses, then:[11]

$$f_w = 1 - \left(\frac{\sigma_1}{\sigma_{1d}}\right)^n \text{ is replaced by}$$
$$f_w = 1 - \frac{\sigma_1}{\sigma_{1D}} \text{ for iterative calculating} \qquad (28)$$

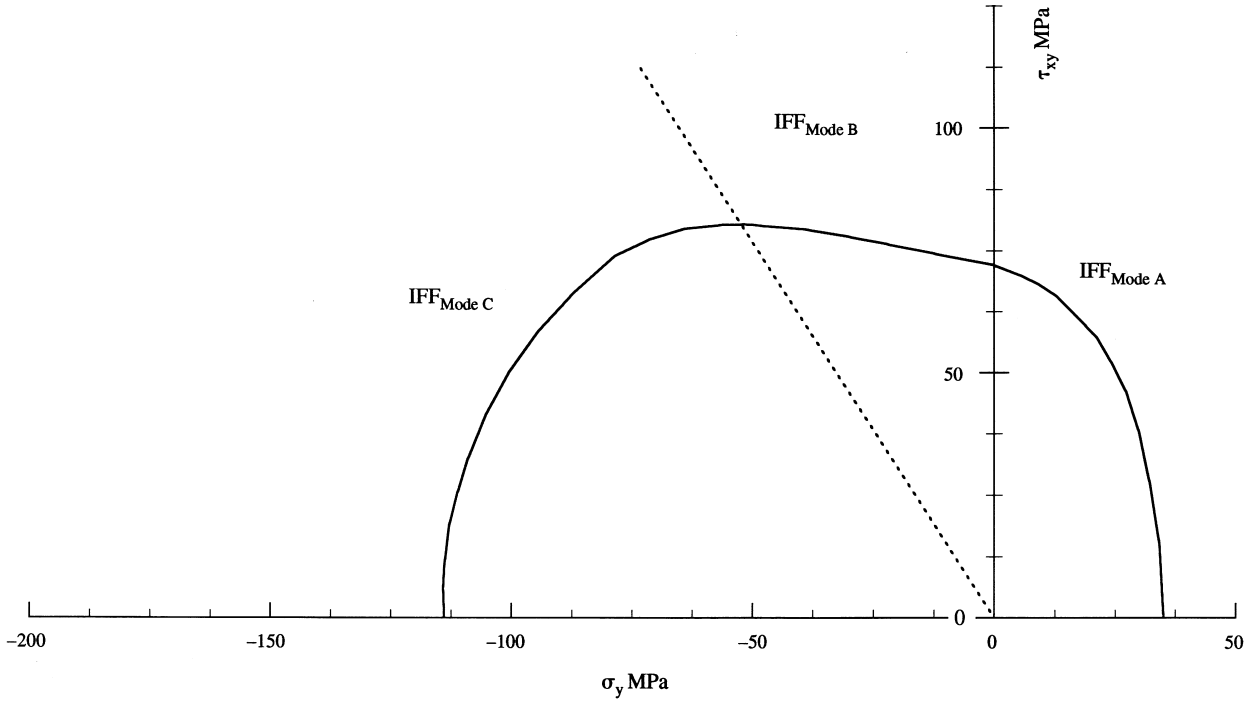

Fig. 10. Biaxial failure stresses of 0° lamina made of GRP material.

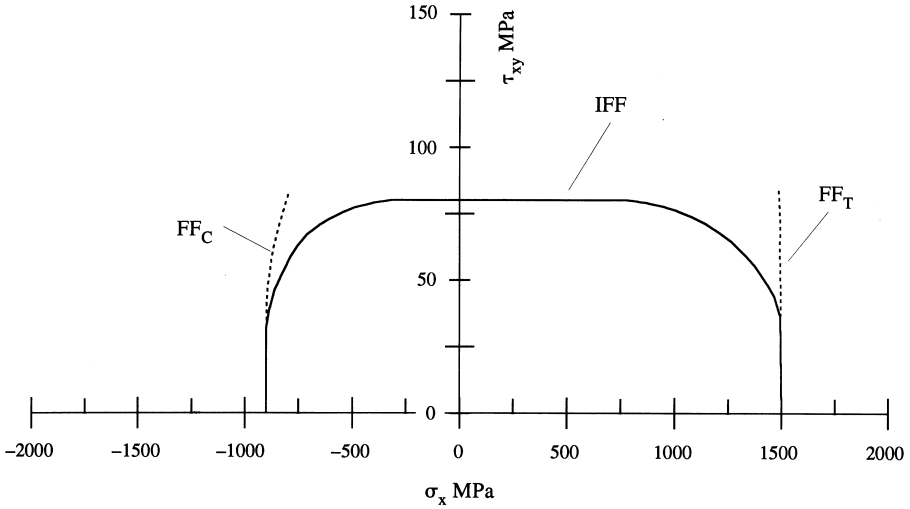

Fig. 11. Biaxial failure stresses of 0° lamina made of CFRP material.

where σ_{1d} ($\approx 1.1X_T$ or $-1.1X_C$, respectively) and n are experimentally determined values, which express quantitatively the degradation d of the fracture resistances R^A of the action plane coming along with σ_1. From our experimental experience, we assume that degradation of the fracture resistances by f_w can only be recognised when σ_1 equals 70% of X or more. To describe this, one needs a large value of the exponent n. For matrices with a relatively high fracture strain, we select $n = 8$, whereas for matrices with a fairly low fracture strain (e.g. 3501-6 epoxy), we choose $n = 6$.

For simplification, the calculation is performed with

$$1 - (0,9 f_{E(FF)})^n \text{ instead of } 1 - \left(\frac{\sigma_1}{\sigma_{1d}}\right)^n$$

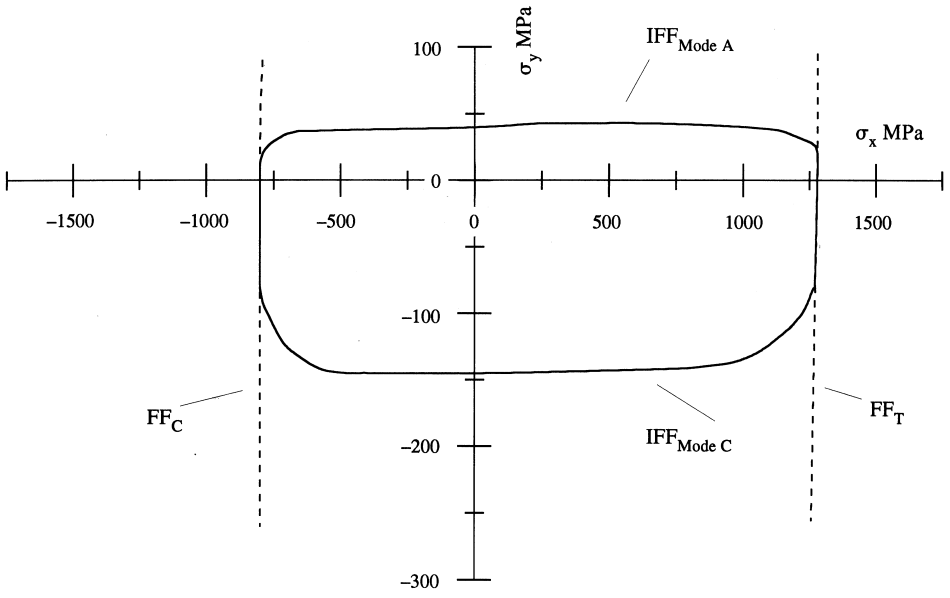

Fig. 12. Biaxial failure stresses of 0° lamina made of GRP material.

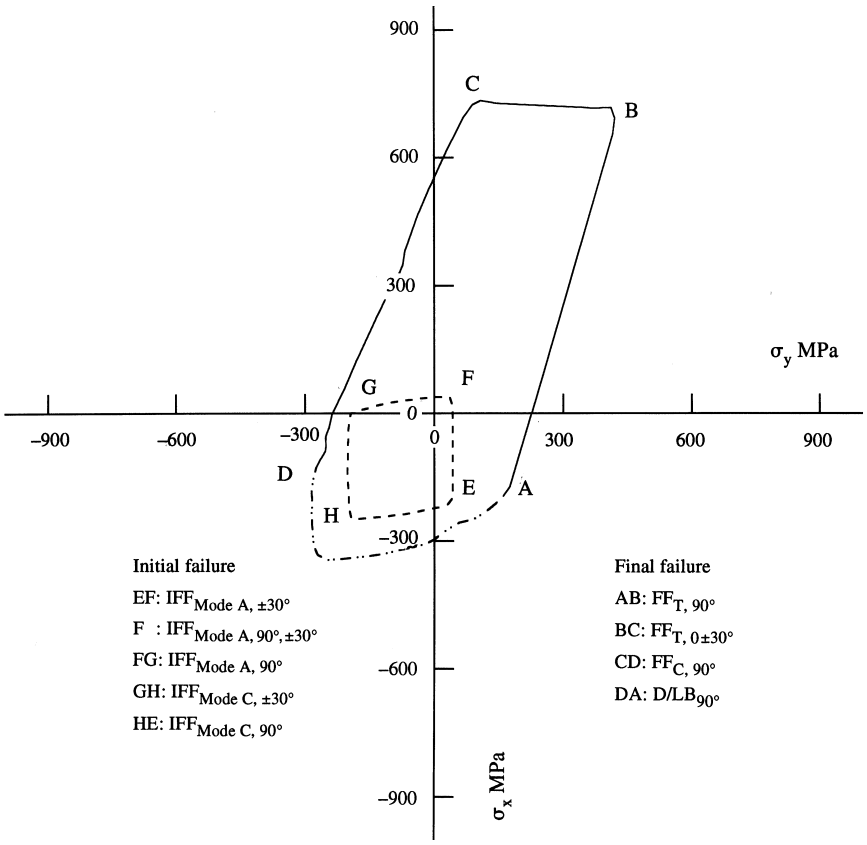

Fig. 13. Biaxial failure stresses of (90°/±30°/90°) laminate made of GRP material.

Even though it is not entirely clear to what extent this is justified, we apply the same degradation for $\sigma_1 > 0$ and $\sigma_1 < 0$ (Table 1) ($\sigma_{1d} > 0$ for $\sigma_1 > 0$ and $\sigma_{1d} < 0$ for $\sigma_1 < 0$).

When the fracture conditions given in Table 1 are exclusively used to distinguish between such states of stress which can be subtained without fracture and states of stress which lead to fracture, the exponent may be $n \neq 1$. If however they are used to calculate the effort $f_{E(IFF)}$, conditions must be kept homogeneous and of first degree in terms of stresses (i.e. the effort value is proportional to the load level). Higher values of n can be taken into account by iterative adaption of the following:

$$\sigma_{1D} \text{ from } 1 - (0,9 f_{E(FF)})^n = 1 - |\frac{\sigma_1}{\sigma_{1D}}|$$

Apart from single fibre breaks, loading the composite with a σ_1 stress always also induces a stress in the matrix acting in the x_1 direction because fibre and matrix are acting as parallel springs. Previous papers[1–4] covered this by a supplementary term $(\sigma_1/\sigma_{1mf})^2$ in the fracture conditions (subscript mf represents matrix failure). However, since we now favour Mohr's fracture hypothesis, we suspect that a matrix stress acting in the fibre direction does not have a noticeable effect on fracture, as long as the strain to failure of the matrix is

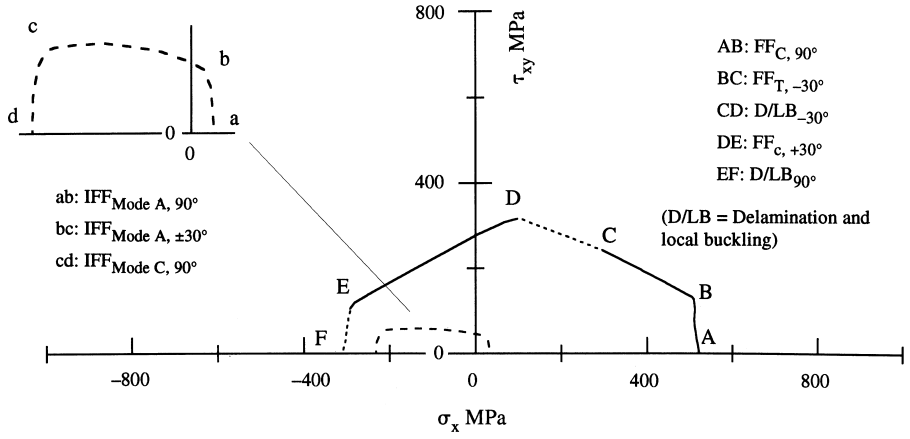

Fig. 14. Biaxial failure stresses of $(90°/\pm 30°/90°)$ laminate made of GRP material.

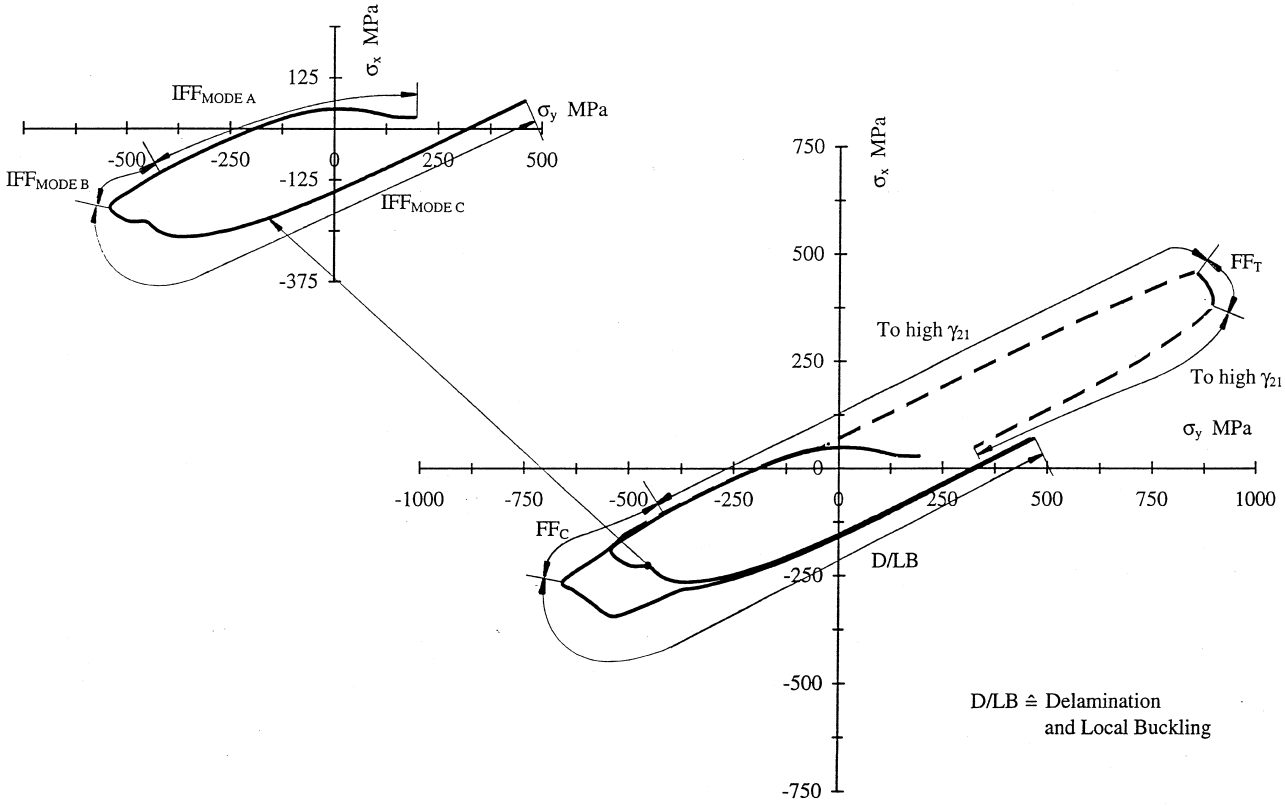

Fig. 15. Biaxial failure stresses of $\pm 55°$ laminate made of GRP material.

considerably higher than that of the fibre. Since this is the case for the composites that are to be analysed in this work, we neglect matrix stresses in the x_1 direction.

7.2 Degradation of elastic quantities after exceeding the crack initiation limits

A degradation method has been described[1] which covers realistically the progressive reduction of certain transverse stiffnesses of the unidirectional ply as a result of increasing crack density. Opening cracks are regarded as if they were 'smeared', and their global effect on the secant moduli E_{2s} and G_{21s} as well as the major Poisson's ratio ν_{12} are described by diminishing all three quantities with a reduction factor η.

When calculating (fictitious) stresses from stress/strain diagrams extrapolated to stresses above the level where uniaxial failure or pure shear failure occurs, and inserting these stresses into the inter-fibre failure conditions, one computes values for the inter-fibre failure effort $f_{E(IFF)}$ which are higher than 1. These fictitious

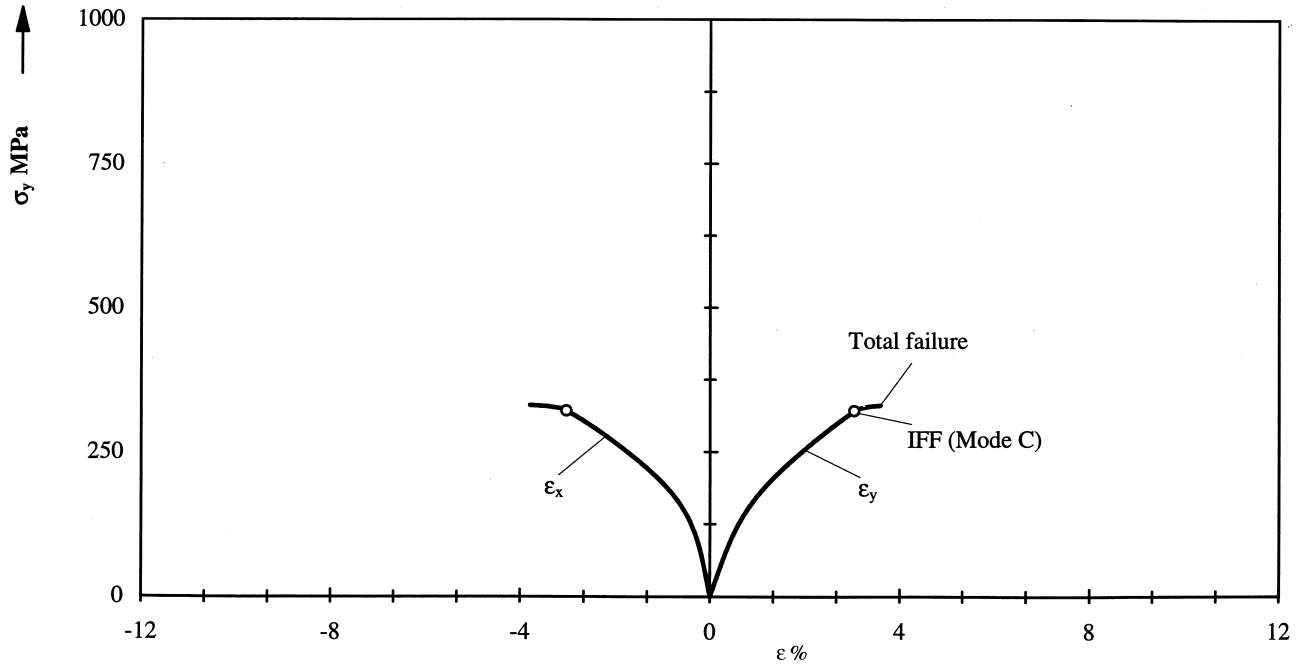

Fig. 16. Stress/strain curves for ±55° laminate made of GRP material ($\sigma_y/\sigma_x = 1/0$).

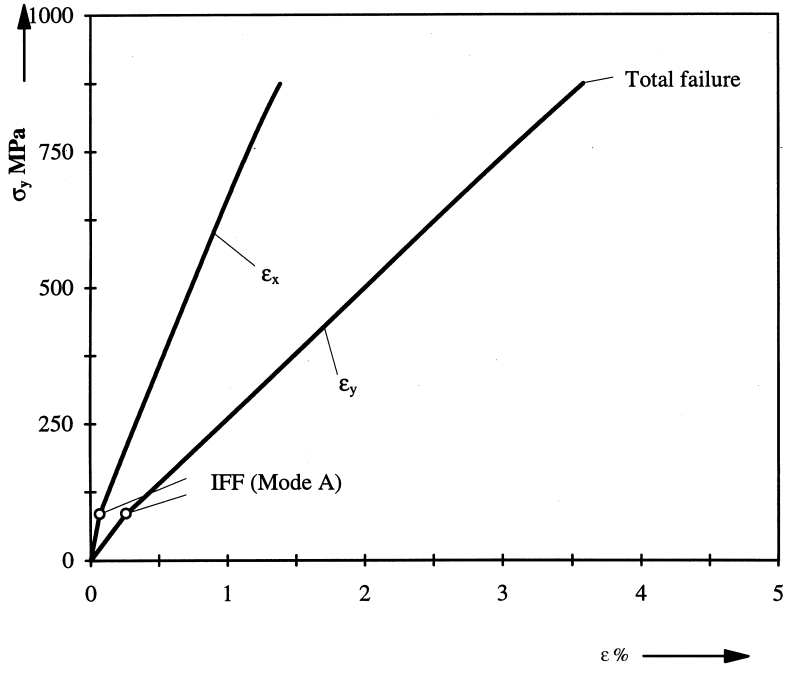

Fig. 17. Stress/strain curves for ±55° laminate made of GRP material ($\sigma_y/\sigma_x = 2/1$).

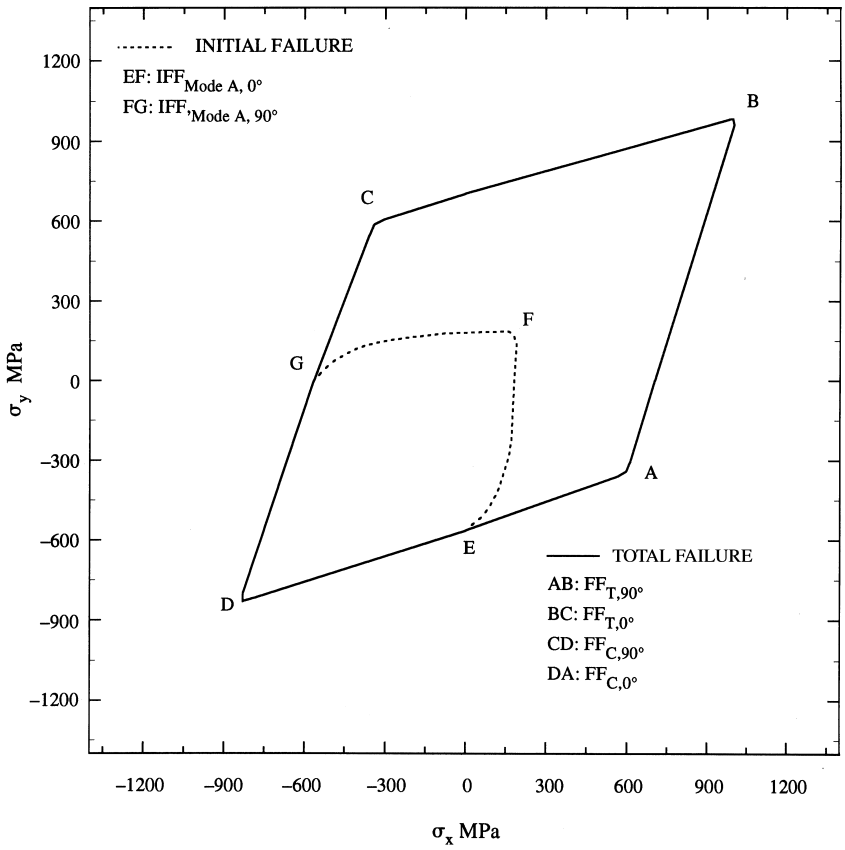

Fig. 18. Biaxial failure stresses for $(0°/\pm 45°/90°)$ laminate made of CFRP material.

effort values $f_{E(IFF)} > 1$ have been used previously[1] as a controlling parameter for the η reduction (see Fig. 8). Since cracks cannot open for $\sigma_2 < 0$ (or more correct $\sigma_n < 0$), only a very small η reduction was designated for this case[1] (see Fig. 8).

The described degradation procedure should build on experimentally deduced curves of $\eta(f_{E(IFF)})$. Because for the composites which are to be analysed here no such experimental values exist, in this paper a self-controlled η reduction is used, which will be explained below.

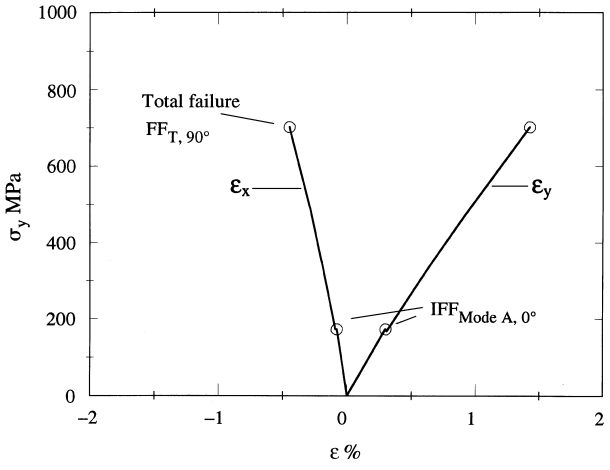

Fig. 19. Stress/strain curves for $(0°/\pm 45°/90°)$ laminate made of CFRP material $(\sigma_y/\sigma_x = 1/0)$.

Furthermore, we distinguish between the fracture modes A, B, and C.

For inter-fibre fracture of Mode A, the secant moduli E_{2s} and G_{21s} evaluated from the stress/strain diagrams (extrapolated if necessary) and the Poisson's ratio ν_{12} are diminished by the same factor $\eta < 1$, which is decreased gradually until the iterative calculation yields $f_{E(IFF)} = 1$ again.

For inter-fibre failure of Mode B and Mode C, the secant modulus E_{2s} is still deduced from the (extrapolated) (σ_2, ϵ_2) curve and not diminished, because the cracked surfaces can still transfer compressive stresses. The Poisson's ratio ν_{12} remains unchanged. Only the secant modulus G_{21s} is reduced by the factor η, until the calculation gives again $f_{E(IFF)} = 1$.

For the self-controlling procedure the calculated $f_{E(IFF)}$ of the affected layer is used by setting $\eta = (f_{E(IFF)})^{-1}$ for each decreasing step.

8 APPLICATION OF DAMAGE ANALYSIS AND FRACTURE ANALYSIS TO FRP LAMINATES

8.1 General procedure

According to the given problem, only the procedure for a load increasing monotonically from zero load to fracture is discussed here. The described calculation models and procedures are utilised by our computer program NOLI FRAN COLAM (non-linear fracture analysis of

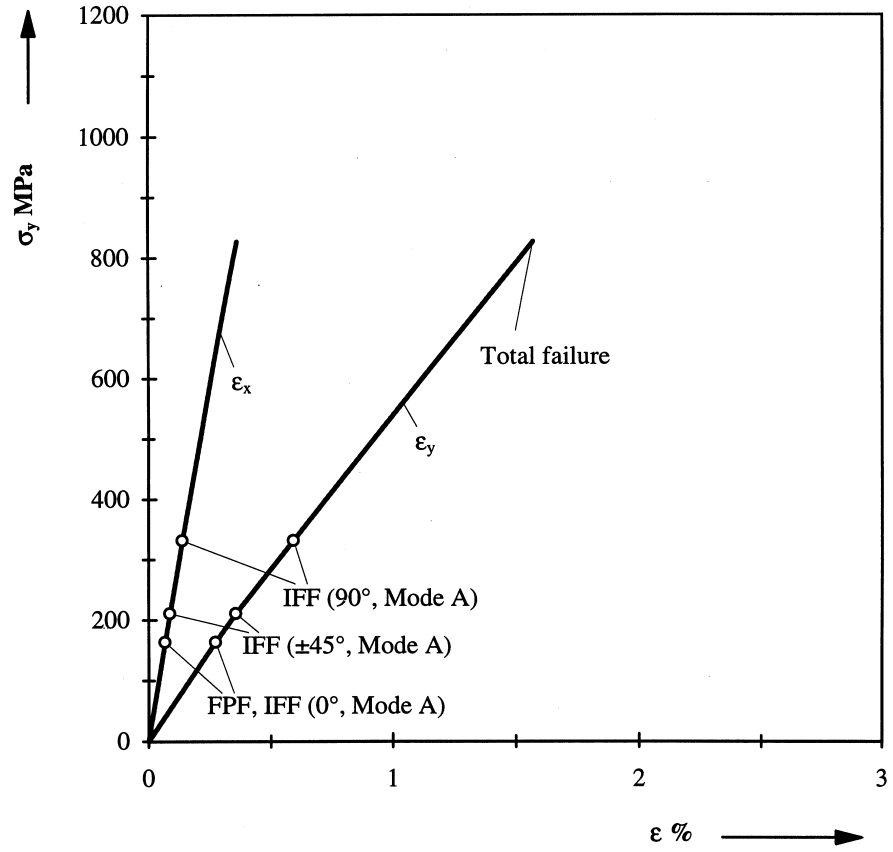

Fig. 20. Stress/strain curves for $(0°/\pm 45°/90°)$ laminate made of CFRP material ($\sigma_y/\sigma_x = 2/1$).

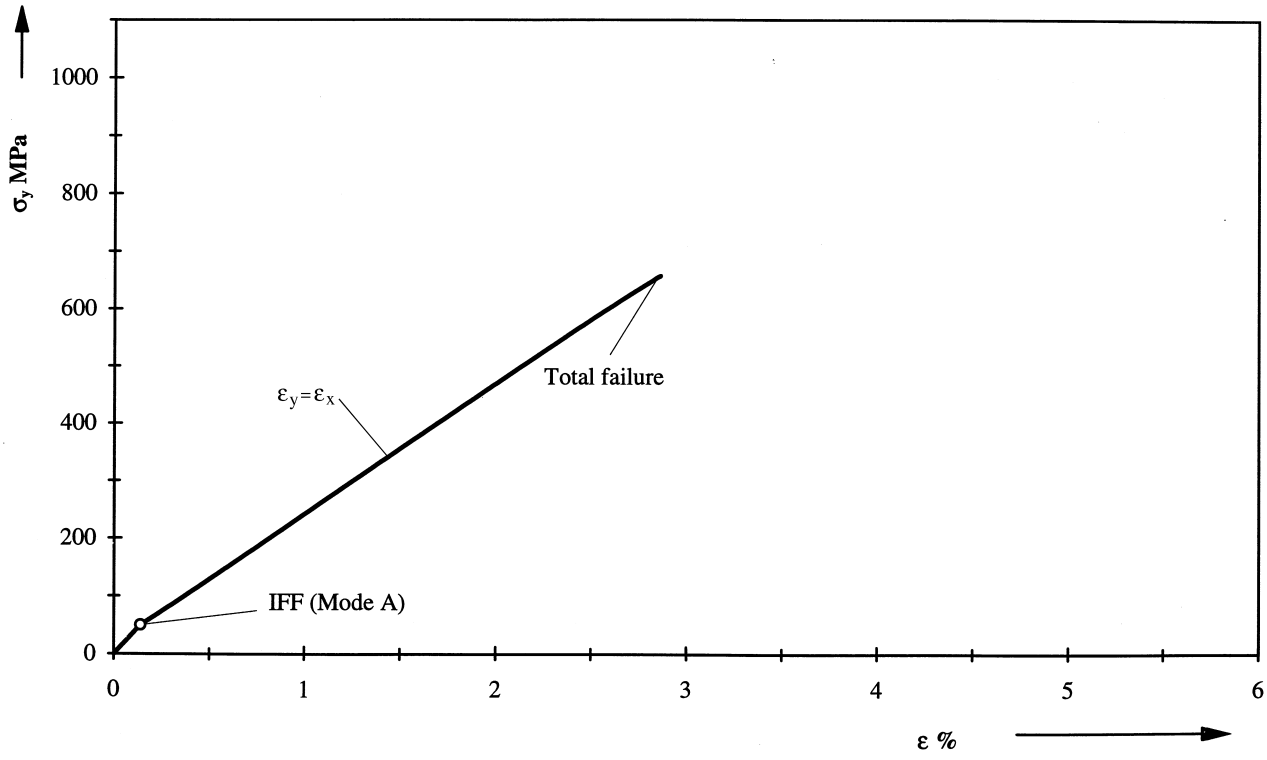

Fig. 21. Stress/strain curves for $\pm 45°$ laminate made of GRP material ($\sigma_y/\sigma_x = 1/1$).

composite laminates). The laminates analysed are described elsewhere.[25]

When manufacturing laminates, residual stresses develop both as a result of shrinkage when curing the matrix, and most of all as a consequence of cooling the laminate after curing at elevated temperatures. However, relaxation takes place with time. Through moisture absorption and the accompanying swelling, residual stresses develop which are of opposite sign, so that the residual stresses caused by cooling the laminate are partially compensated for. Since no further details are given about the laminates in this problem, we account for this effect by assuming that at the onset of loading, the residual stresses are already reduced to 50% compared to the level they had immediately after cooling.

Whenever the calculation is performed using elasticity quantities which have been reduced by η, the residual stresses are re-calculated with the reduced quantities for every load level (because of the stiffness loss which accompanies crack formation, the residual stresses are reduced[11]).

In any case, after crack initiation in the first affected ply, increasing the load has to be carried out in small increments. However, the crack initiation threshold itself can in principle be reached with one large step by the help of iterations. Nevertheless, if the goal is to predict the stress/strain diagrams of the laminates by computation, increasing the load has to be executed in small load steps from the beginning.

The deterioration of unreasonably designed laminates (which are— according to netting analysis—not able to transfer load, e.g. a $\pm 55°$ tube under axial tension), which progresses rapidly after crack initiation, cannot be represented correctly by means of calculation. In this case, we compute with large deformations (geometrically non-linear). When they exceed a limiting value ($\gamma_{21} \geq 0{\cdot}2$), calculation is cancelled.

8.2 Interpretation of the computed results

A reliable interpretation and evaluation of the computational result that an inter-fibre failure limit is exceeded is achieved not only by indicating the related stresses, but also the fracture mode (A, B, C).

Least critical for a laminate is progressive crack formation after Mode A. Particularly when the crack formation is caused essentially by transverse tensile stresses, cracks open at an angle of $\theta_{fp} = 0°$ which to some extent removes load from the affected ply.

Such a load removal is only partly possible in Mode B. Only the shear modulus G_{21s} is reduced, and not E_{2s}. Thus, after exceeding the crack initiation limit, high σ_2 compressive stresses quickly build up when the load is increased further. The fracture point moves to the left on the (σ_2, τ_{21}) fracture envelope, i.e. the fracture mode may change from B to C.

Fracture in Mode C can be extremely dangerous for the laminate, especially when through a dominating compressive stress $(\sigma_2 >> \tau_{21})$ a fracture angle θ_{fp}

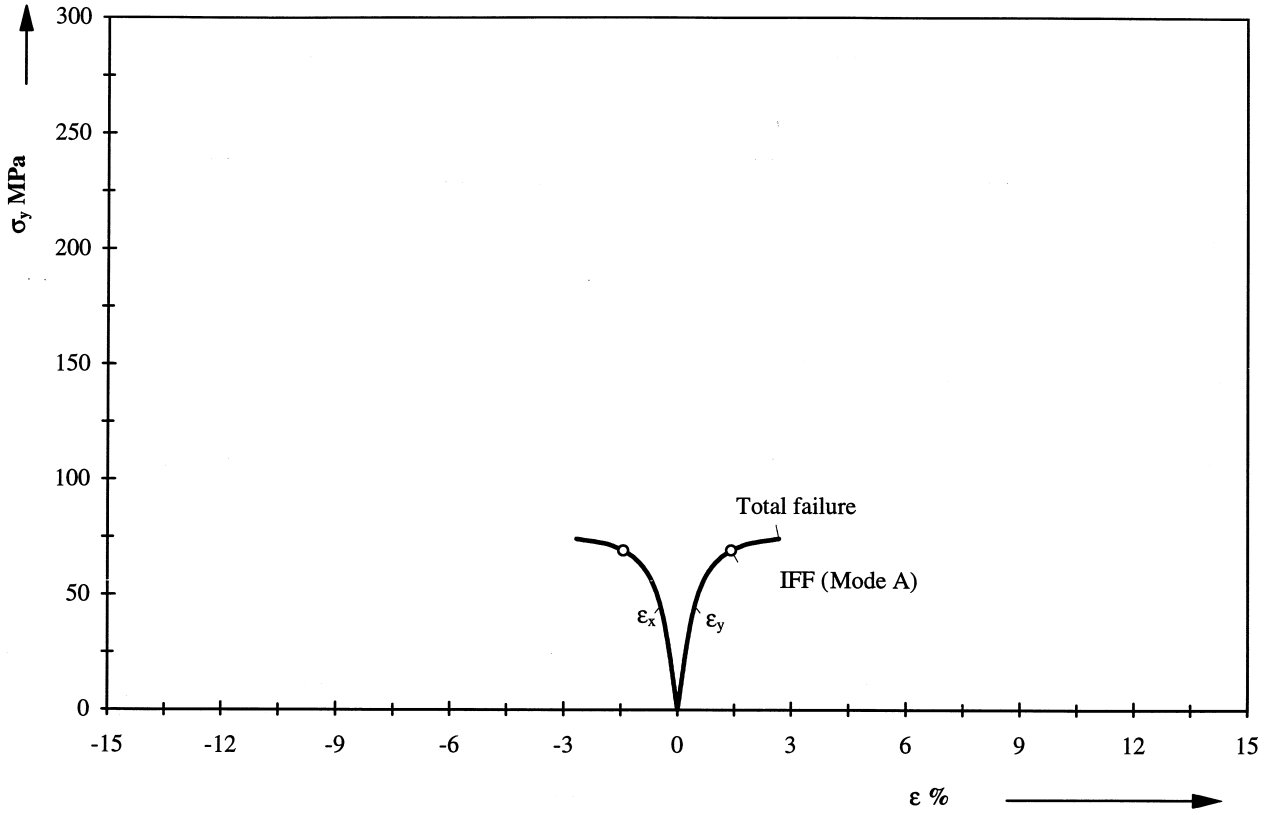

Fig. 22. Stress/strain curves for $\pm 45°$ laminate made of GRP material ($\sigma_y/\sigma_x = 1/-1$).

between 30° and 55° results. The inclined fracture planes plus the effect of the high σ_2 compressive stress which is still acting constantly cause a wedge effect. When the frictional resistance on the originated inclined plane is overcome, one side of the broken layer tends to push its way over the other part gliding on the fracture plane, so that it 'climbs up' in the thickness direction (see Fig. 9). This has an explosive effect on the laminate, which may lead to local delaminations and subsequent buckling of neighbouring layers when further increasing the load. Of course, how critical these delaminations are is dependent on the local parameters (layer thickness, fibre direction, affected layer being inside or on the surface of the laminate, etc.). Thus, the results of the stress and fracture analysis can at first hand only point out the risks and lead to a more detailed examination of the local situation or, if possible, to a re-design of the laminate to avoid reaching this critical situation.

Our newly developed fracture criteria with fracture angle determination allow a numerical prediction when a critical explosive effect can be anticipated for a laminate. As soon as inclined fracture occurs at an angle $\theta_{fp} \neq 0°$, the shear stress τ_{nt} which is needed to satisfy force equilibrium in the fracture plane is not transferred any more by the material. At the very most, it might be (entirely or partially) replaced by a 'frictional stress' $\mu\sigma_n$. A critical situation develops as soon as

$$\mu|\sigma_n| \leq |\tau_{nt}| \tag{29}$$

because then both fracture planes start to slide on each other, if that is not prevented by vertical supporting forces of the neighbouring layers. How long the laminate withstands the explosive effect depends on its particular stacking sequence.

We cancel calculation as soon as

$$|\tau_{nt}| = \frac{1}{2}|\sigma_2 \sin 2\theta_{fp}| \geq 3\mu|\sigma_n| \tag{30}$$

with

$$\theta_{fp} = \arccos\left(\frac{f_w R^A_{\perp\perp}}{-\sigma_2}\right)^{\frac{1}{2}}$$

because now, a severe delamination and buckling risk can be expected.

When designing a heavily loaded GRP torsion tube spring for a passenger car,[22,23] it was learned that only

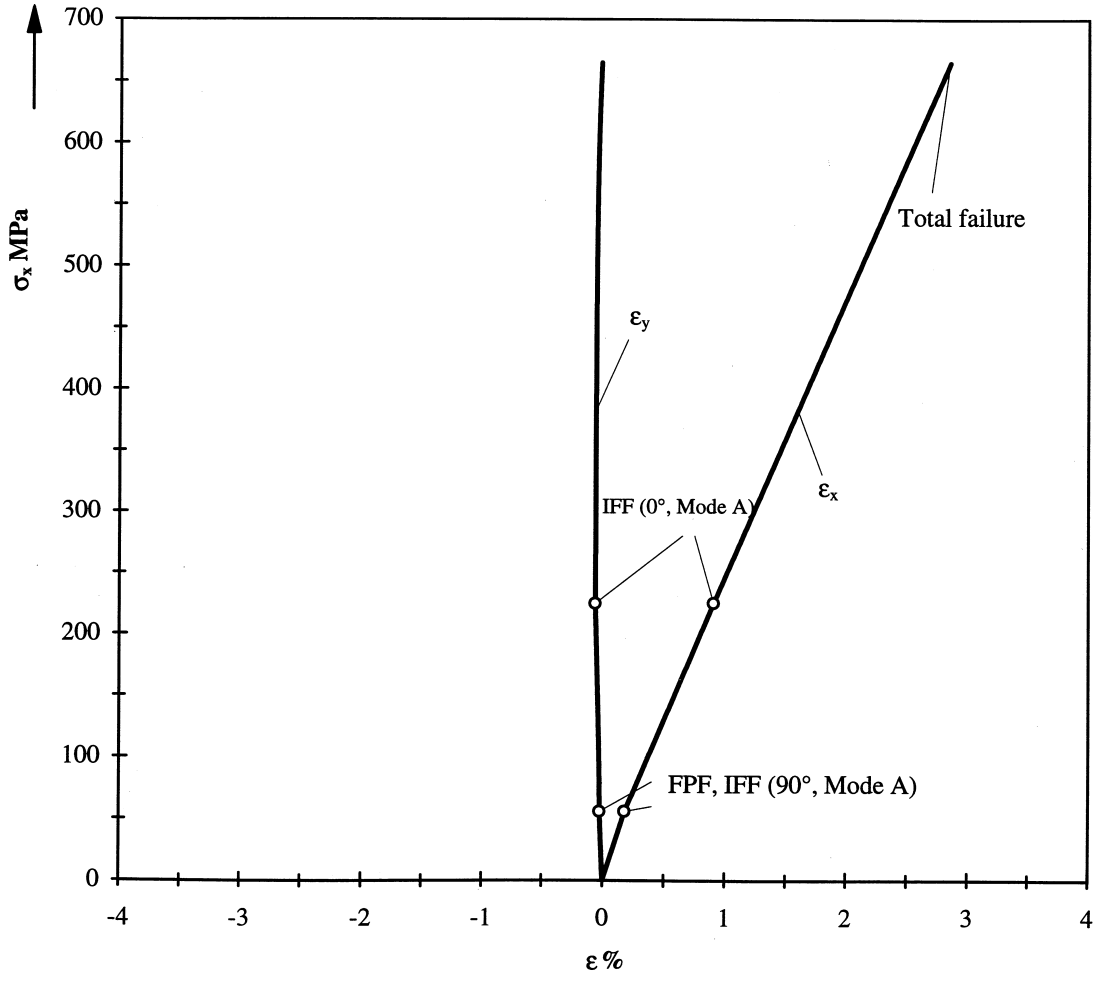

Fig. 23. Stress/strain curves for 0°/90° GRP laminate ($\sigma_y/\sigma_x = 0/1$).

one single inclined fracture event of this kind may lead to ultimate failure of the structural member. The wall of the torsion spring consisted of two unidirectional layers with $+45°$ and $-45°$ fibre orientation, respectively, and one intermediate crack arresting ply. The thicker outer layer experienced stresses $\sigma_1 > 0$ and $\sigma_2 < 0$. At load cycles of about $N \approx 2 \times 10^6$, the σ_2 compressive stress caused an inclined wedge-shaped fracture at an angle of $\theta_{fp} \approx \pm 55°$, which lead to the final collapse of the twisted GRP tube through the development of radial forces. This kind of failure is explained in more detail elsewhere.[11]

9 THEORETICAL RESULTS

The theory described above was applied to predict the behaviour of laminates supplied by the organizers.[25] In the analysis, the lamina properties of the four materials (T300/914C, AS4/3501-6, E-glass/MY750 epoxy and E-glass/LY556 epoxy) investigated were taken from the data provided.

Figure 10 shows the failure envelope for the E-glass/LY556 unidirectional lamina subjected to combined transverse and shear loading (σ_y,τ_{xy}). Three modes of failure are predicted depending upon the state of stresses in the lamina. Under combined transverse tension and shear, the failure mode is IFF (Mode A); under moderate transverse compression it is IFF (Mode B) and at fairly large transverse compressive loading it is IFF (Mode C).

Figure 11 shows the failure envelope for the T300/914C lamina subjected to combined longitudinal and shear loading (σ_x,τ_{xy}).

Figure 12 shows the failure envelope for the E-glass/MY750 epoxy lamina subjected to combined direct loading (σ_x,σ_y). Four modes of failure are predicted, namely IFF (Mode A), IFF (Mode C), FF_T and FF_C. Each mode operates in different regions which are indicated.

Figures 13 and 14 show the failure envelopes of the $90°/\pm 30°/90°$ E-glass/LY556 epoxy laminate under combined direct loading (σ_y,σ_x) and combined direct stress and shear loading (σ_x,τ_{xy}), respectively. Both initial and final failure envelopes are shown. Different modes of failure operate at different portions of the initial and final failure envelopes as indicated on the figures.

Figure 15 shows the failure envelope for the $\pm 55°$ E-glass/MY750 epoxy laminate subjected to a variety of biaxial direct stresses (σ_y,σ_x). Initial and final failure stresses are shown.

The predicted stress/strain curves for $\pm 55°$ E-glass/epoxy laminate under uniaxial loading ($\sigma_y/\sigma_x = 1/0$) and biaxial loading ($\sigma_y/\sigma_x = 2/1$) are shown in Figs 16 and 17.

Figure 18 shows the predicted failure envelope for the $0°/\pm 45°/90°$ quasi-isotropic laminate under biaxial direct stresses (σ_y,σ_x). It is remarkable that in the compression quadrant only FF occurs.

Figures 19 and 20 show the predicted stress/strain curves under uniaxial ($\sigma_y/\sigma_x = 1/0$) and biaxial ($\sigma_y/\sigma_x = 2/1$) loading for the $0°/\pm 45°/90°$ quasi-isotropic laminate made of AS4/3501-6 material.

Biaxial stress strain curves for the $\pm 45°$ E-glass/MY750 epoxy laminate are shown in Figs 21 and 22 for two loading cases: ($\sigma_y/\sigma_x = 1/1$) and ($\sigma_y/\sigma_x = 1/-1$).

Finally, the behaviour of $0°/90°$ E-glass/MY750 epoxy laminate under uniaxial tensile loading $\sigma_y/\sigma_x = 1/0$ is predicted in Fig. 23. The laminate fails in three stages. In the first stage the $90°$ plies fail in IFF (Mode A) as FPF. This is followed by failure of the $0°$ plies in IFF Mode A and finally total failure of the laminate.

10 CONCLUDING REMARKS

The introduction of new inter-fibre fracture criteria, which are based on the brittle failure behaviour of composites, makes fracture analysis even more realistic than it has been with the methods described previously.[1] In addition, the new criteria make a distinction between different fracture modes (A, B and C) possible.

Furthermore, application of separate fracture criteria for fibre failure and inter-fibre fracture provides a rapid overview of the fractures which can be expected for a laminate. This can be achieved by neglecting the η degradation of the elastic quantities when running the calculation program the first time (especially for CFRP, the effect of the η degradation is fairly small anyway).

It is still not known for sure how much the *thin layer effect* and the *in situ* effect have to be taken into consideration, i.e. the fact that crack formation in very thin layers is delayed when they are embedded between stiff neighbouring plies.[12] Moreover, the notch effect inter-fibre fractures have on the fibres of neighbouring layers should be covered by introducing a stress concentration factor. However, since no reliable findings concerning these questions are available and the results of our work should be comparable to the results of other authors, we excluded correction factors accounting for these effects from this paper.

We are strongly convinced that the Failure Analysis Exercise initiated in the UK will have a major impact on the development of this domain which has been abandoned for a long time, provided that the experience gained in different research fields can be taken into account.[24]

ACKNOWLEDGEMENTS

The authors would like to thank Mrs Professor Dr R. Jeltsch-Fricker, Kassel, for discussion of mathematical

aspects and Dr-Ing. D. Huybrechts, Aachen, for discussion of engineering aspects. The skillful typing of Mrs M. Streb is gratefully acknowledged. Thanks are due to Dipl.-Ing. S. Wenzel for computation and to Dipl.-Ing. A. Knickrehm for translation of the manuscript.

REFERENCES

1. Puck, A., Calculating the strength of glass fibre/plastic laminates under combined load. *Kunststoffe, German Plastics*, 1969, **55**, 18–19 (German text pp. 780–787).
2. Puck, A. and Schneider, W., On failure mechanisms and failure criteria of filament-wound glass-fibre/resin composites. *Plast. Polym.*, 1969, **Feb.**, 33–43.
3. Puck, A., Fracture criteria for highly stressed fibre–plastic composites which meet requirements of design practice. *Kunststoffe, German Plastics*, 1992, **82**, 34–38 (German text pp. 149–155).
4. Puck, A., Should fibre–plastics composites be designed with strain or stress criteria? *Kunststoffe, German Plastics*, 1992, **82**, 34–36 (German text pp. 431–434).
5. Puck, A., A failure criterion shows the direction. *Kunststoffe, German Plastics*, 1992, **82**, 29–32 (German text pp. 607–610).
6. Michaeli, W. and Huybrechts, D., A new approach for the dimensioning of thick laminates using physically based strength criteria. In *Proc. 39th Conf. of the Society for the Advancement of Material and Process Engineering (SAMPE)*, Vol. 2, 11–14 April 1994, Anaheim, CA, pp. 2829–2840.
7. Michaeli, W. and Huybrechts, D., A new approach for the dimensioning of thick laminates. In *International Mechanical Engineering Congress (IMECE) of the American Society of Mechanical Engineers (ASME)*, Vol. 49, 6–11 Nov. 1994, Chicago, IL, pp. 307–319.
8. Cuntze, R. G., Evaluation and application of a new, physically based 2D/3D inter-fibre-fracture (IFF) strength criterion. In *Proc. Int. Symp. on Advanced Materials for Lightweight Structures, ESTEC*, March 1994, Noordwijk (ESA-WPP-070), pp. 133–139.
9. Huybrechts, D. and Michaeli, W., Dimensioning of thick laminates: New IFF strength criteria based on the determination of the fracture plane, experiments for verification. In *16th Conf. of the European Chapter of the Society for the Advancement of Material and Process Engineering (SAMPE)*, 30 May–1 June 1995, Salzburg, Austria, pp. 211–222.
10. Kroll, L. and Hufenbach, W., New proof of laminate design by a physically based failure criterion. In *Proc. ICCM-10*, Vol. 1, ed. A. Poursatrip and K. Street. August 1995, Vancouver, Canada, pp. 715–720.
11. Puck, A., *Festigkeitsanalyse von Faser-Matrix-Laminaten, Modelle für die Praxis (Strength Analysis of Fibre-Matrix/Laminates, Models for Design Practice)*. Carl Hanser Verlag, Munich, Germany, 1996.
12. Talreja, R. (ed.), *Damage Mechanics of Composite Materials*. Elsevier, Amsterdam, 1994.
13. Schürmann, H., *Zur Erhöhung der Belastbarkeit von Bauteilen aus Faser-Kunststoff-Verbunden durch gezielt eingebrachte Eigenspannungen (How to Increase the Load Bearing Capacity of Fibre-Plastic Composite Components by the Introduction of Internal Stresses)*. Fortschritt-Berichte VDI, Reihe 1, Nr. 170, VDI-Verlag Düsseldorf, Germany, 1989.
14. Rosen, B. W., Mechanics of composite strengthening. In *Fibre Composite Materials*. American Society for Metals, 1995, pp. 37–76.
15. Edge, E. C., Does transverse and shear loading affect the compression strength of unidirectional CFC? A reply to Dr Hart-Smith. *Composites*, 1994, **25**, 159–164.
16. Parry, T. V. and Wronski, A. S., Kinking and compressive failure in unaxially aligned carbon fibre tested under superimposed hydrostatic pressure. *J. Mater. Sci.*, 1982, **17**, 893–900.
17. Hart-Smith, L. J., Fibrous composite failure criteria—Fact and fantasy. In *7th Int. Conf. on Composite Structures*, Paisley, UK, July 1993. McDonnell Douglas MDC 93 K0047.
18. Mohr, O., Welche Umstände bedingen die Elastizitätsgrenze und den Bruch eines Materials? (Which circumstances are causing yield limit and fracture of a material?). *Civilingenieur*, 1900, **44**, 1524–1530 and 1572–1577.
19. Hashin, Z., Failure criteria for unidirectional fiber composites. *J. Appl. Mech.*, 1980, **47**, 329–334.
20. Puck, A., Physically based 3D fracture criteria for unidirectional composites. *Presentation at the Working Group* 'New Fracture Criteria', Kassel University, AG Ing. Math., June 1993.
21. Paul, B., A modification of the Coulomb–Mohr theory of fracture. *J. Appl. Mech.*, 1961, **2**, 259–268.
22. Puck, A., Torsion tube springs to replace highly stressed steel springs. *Kunststoffe, German Plastics*, 1990, **80**, 27–30 (German text pp. 1380–1384).
23. Garbe, J. and Puck, A., Experience with criteria for fracture of FRP torsion springs in cyclic loading. *Kunststoffe, German Plastics*, 1993, **83**, 28–31 (German text pp. 406–411).
24. Hinton, M. J. and Soden, P. D., Predicting failure in composite laminates: the background to the exercise. *Compos. Sci. Technol.*, 1998, **58** (7), 1001.
25. Soden, P. D., Hinton, M. J. and Kaddour, A. S., Lamina properties, lay-up configurations and loading conditions for a range of fibre reinforced composite laminates. *Compos. Sci. Technol.*, 1998, **58** (7), 1011.

APPENDIX

Discussion of difficulties with nomenclature and symbols for "Reserve Factor" and "Effort"

In the anglo-american aerospace literature, the symbol *RF* is used for the Reserve Factor. Since that can also mean the product between *R* and *F*, we substituted with f_{Res} or the short form (in recent publications) f_{R}.

In the German literature, the term "Anstrengung" is preferred. All possible translations (effort, exertion, stress exposure factor, exploitation factor) are not completely satifactory. However, we decided to use "effort" as the shortest term, symbolised by the letter E in calligraphic style ($\mathcal{E}$). Unfortunately, this is often mixed up with epsilon (ε). To avoid that, we use the symbol f_{E} instead in our most recent publications, which also emphasises the close relation to the Reserve Factor f_{R}; both are dimensionless factors. In the absence of internal stresses, it is $f_{\mathrm{E}} = (f_{\mathrm{R}})^{-1}$.